The staphylococcal type VII secretion system impacts daptomycin sensitivity through controlling bacterial cell envelope integrity

Victoria Smith[1], Giridhar Chandrasekharan[1], Kate E. Watkins[1], Ramon Garcia Marset[1$], Jeannifer Yap[2], Sebastien Perrier[3], Arnaud Kengmo Tchoupa[1+], and Meera Unnikrishnan[1*].

1. Division of Biomedical Sciences, Warwick Medical School, University of Warwick, Coventry, CV4 7AL, UK.
2. Department of Chemistry, University of Warwick, Coventry, CV4 7AL, UK
3. Department of Chemistry and Warwick Medical School, University of Warwick, Coventry, CV4 7AL, UK.

$ current address: Centre for Urological Biology, Division of Medicine, University College London, WC1E 6BT London, UK.

+ current address: Cluster of Excellence EXC 2124 Controlling Microbes to Fight Infections, University of Tübingen, 72076 Tübingen, Germany

*Corresponding author m.unnikrishnan@warwick.ac.uk

Key words: Type VII secretion system, membrane integrity, membrane fluidity, daptomycin,

Summary

The *Staphylococcus aureus* type VII secretion system (T7SS) plays an important role in bacterial virulence during infection. However, T7SS functions during infection and in bacterial physiology are poorly understood. Here, we demonstrate that *S. aureus* strains lacking the T7SS transporter EssC or effectors, EsxC and EsxA, were highly sensitive to the important last resort drug, daptomycin. T7SS mutants displayed decreased membrane fluidity, altered cell membrane protein localisation, distinct cell surface morphologies, with effects on cell wall synthesis as well as surface charge under normal growth conditions, indicating that the T7SS is critical to cell envelope function. Daptomycin binding was enhanced in the mutants, whose membranes were more permeable when treated with the drug. Furthermore, the lack of EsxC enhanced daptomycin sensitivity during intracellular infection and during murine skin infection. Thus, our data show that the staphylococcal T7SS impacts sensitivity to membrane-acting drugs through modulating membrane integrity, indicating its potential as a drug target.

Keywords: Type VII secretion system, cell membrane integrity, membrane fluidity, daptomycin, intracellular infection

53 **Introduction**

54 *S. aureus* is a highly versatile pathogen and a commensal bacterium which causes infections in
55 both humans and animals. Staphylococcal infections can be nosocomial or community-acquired,
56 and can range from mild skin abscesses to severe life-threatening infections including septic shock
57 and bacteraemia[1]. *S. aureus* infections place a huge cost burden on healthcare sectors across
58 the world, especially due to the occurrence of antibiotic-resistant strains, such as methicillin-
59 resistant *S. aureus* (MRSA) and strains with varying levels of vancomycin resistance[2,3]

60

61 *S. aureus* possesses an array of surface and secreted factors that help the bacterium colonise the
62 host and establish an infection[4]. One such virulence-associated factor is the type VII secretion
63 system (T7SS), which is widely found in Gram positive bacteria[5]. The T7SSb in *S. aureus* and
64 other firmicutes is distinct from the systems in mycobacteria (T7SSa) although both are
65 characterised by WXG containing small substrates such as EsxA and EsxB[6,7]. The T7SS in *S.*
66 *aureus* is modular in nature, with heterogenous expression between strains[8,9]. Typically, in
67 commonly studied *S. aureus* strains including USA300, Newman and RN6390, the T7SS locus
68 comprises integral membrane proteins (EsaA, EssA, EssB and EssC), cytosolic proteins (EsaB
69 and EsaG), several secreted substrates (EsxA, EsxB, EsxC, EsxD and EsaD) and chaperones
70 (EsaE)[7,10]. EssC is the central transporter which is responsible for export of substrates and co-
71 dependent export of secreted substrates has been demonstrated[6,11]. While specific interactions
72 between the different T7SS components have been described, the overall structure of the
73 secretion apparatus is poorly defined for the *S. aureus* T7SS[10,11]. Assembly of a functional system
74 is dependent on the membrane microdomain protein, flotillin A (FloA)[12].

75

76 Recent studies have reported a role for T7SS in modulation of intraspecies competition. A T7SS
77 substrate EsaD with nuclease activity mediates killing of *S. aureus* strains that lack the anti-toxin
78 EsaG[13]. An LXG-domain containing protein, TspA, encoded distally to the T7SS cluster shows

79 T7SS-dependent toxic activity, which was neutralized by an antitoxin TsaI[14]. Some substrates
80 modulate host interactions during infection; EsxA modulates host cell death and EsaE elicits
81 cytokine production during infection[15,16]. However, substrates of this system are yet to be defined
82 in many *S. aureus* strains and specific functions of effectors remain elusive.
83
84 T7SS in other bacterial species has been described to support bacterial functions like DNA
85 transfer, membrane integrity and spore development, although for *S. aureus*, it is not clear if T7SS
86 is important in staphylococcal physiology[17-19]. Our recent study on the T7SS substrate EsxC and
87 the transporter EssC showed that mutants lacking these proteins were more sensitive to
88 unsaturated host-derived fatty acids[20]. T7SS defects compromised membrane integrity and
89 induced oxidative stress in presence of antimicrobial fatty acids, indicating a role for these proteins
90 in membrane homeostasis. Here we report that the absence of T7SS causes an increased
91 sensitivity to membrane targeting drugs like daptomycin, both during infection *in vitro* and *in vivo*.
92 We further demonstrate distinct effects on cell surface morphology, membrane fluidity, charge and
93 protein localization in T7SS transporter and substrate mutants indicating a role for T7SS in
94 controlling membrane integrity. Our data suggest that targeting the T7SS could augment activities
95 of membrane-acting drugs like daptomycin.
96
97 **Results**
98 **T7SS mutants are more sensitive to membrane-acting drugs**
99 The cyclic lipopeptide antibiotic, daptomycin, is a key drug used to treat resilient *S. aureus*
100 infections. Daptomycin binds to the cell membrane in a calcium-dependent manner[21]. As our
101 previous studies indicated a potential impact of T7SS on membrane homeostasis[20], we
102 investigated whether the *S. aureus* USA300 JE2 mutants lacking either the substrate EsxC
103 (Δ*esxC)* or the central T7SS transporter EssC, (Δ*essC)* respond differently to membrane-acting
104 drugs like daptomycin. Growth of T7SS mutants were compared to the WT USA300 JE2 strain in

105 the presence or absence of daptomycin. When cultured in presence of 5 μg/ml daptomycin, growth
106 of the WT USA300 JE2 strain is delayed, but growth of Δ*esxC* and Δ*essC* was significantly
107 impaired compared to the WT (Fig. 1 A, B). No differences were seen between the strains in growth
108 rates in tryptic soy broth (TSB) without antibiotic (Fig. S1 A). Further, a 10-fold decrease in colony
109 forming unit counts for the mutants was also observed in the presence of daptomycin (Fig. 1 C).
110 When Δ*esxC* was complemented with a plasmid containing the *esxC* gene, the phenotype of the
111 WT was restored (Fig. 1 D, E). To investigate if other effectors had similar effects, we studied a
112 strain lacking another T7SS substrate, EsxD[11]. However, the deletion of *esxD* in USA300 JE2
113 strain did not result in any growth defects in the presence of daptomycin (Fig. S2 A, B). The T7SS
114 mutants Δ*esxC* and Δ*essC* were also found to be more sensitive to daptomycin in comparison to
115 the WT in a killing assay where logarithmic phase bacteria were treated for 2 h with daptomycin
116 (Fig. 1 F, G).
117
118 We investigated the effect of T7SS on daptomycin sensitivity in other strain backgrounds. The
119 growth of RN6390 *S. aureus* was impacted more by the addition of daptomycin, with the bacterial
120 growth initiating much later (~14 h) compared to the USA300 JE2 strain (~8 h). However, a similar
121 trend was seen in the growth of mutants; Δ*esxC* and Δ*essC* mutants were more susceptible than
122 the WT to treatment with daptomycin (Fig. S2 C, D). A defect in growth was also seen in USA300
123 LAC Δ*esxA* mutant, while Δ*esxB* appeared to grow similar to the WT (Fig. S2 E, F) The Newman
124 strain was also more sensitive than USA300 JE2 to daptomycin with growth being delayed until
125 around 14 h. There was less difference between WT and the Δ*esxA* mutant however a similar
126 trend was observed (Fig. S2 G, H).
127
128 To determine if the differences observed between the WT and T7SS mutants were limited to
129 daptomycin, other membrane-targeting antimicrobials, such as gramicidin and bithionol, were
130 tested. Gramicidin is a polypeptide antimicrobial peptide that forms ion channels in the cell

131 membrane allowing diffusion of monovalent ions such as potassium (K^+) and sodium (Na^+),
132 disrupting cell ion concentrations[22]. Bithionol is an inhibitor of soluble adenylyl cyclase and its
133 membrane-disrupting activity was associated with its ability to kill *S. aureus* persister cells[23]. When
134 treated with 2 µg/ml gramicidin, the WT JE2 strain did not have any growth defects, however the
135 T7SS mutants displayed a slower growth (Fig. 1 H). A similar defect in growth was also seen in
136 the presence of biothionol, although the Δ*esxC* and Δ*essC* mutant showed only a slightly slower
137 growth in the presence of 1 µg/ml bithionol (Fig. 1 I). Finally, this effect appears to be specific to
138 membrane-acting drugs as other drugs which target the cell wall (vancomycin, oxacillin) or DNA
139 replication (ciprofloxacin, mitomycin) did not differentially affect the growth of T7SS mutants as
140 compared to the WT (Fig. S3).
141

142 **Δ*esxC* displays decreased membrane fluidity**

143 Changes in membrane fluidity can affect membrane function and antibiotic sensitivity. We probed
144 T7SS effects on the membrane by assessing membrane fluidity of the WT and Δ*esxC* mutant.
145 Pyrene decanoic acid, an excimer-forming lipid[24], was employed to measure the fluidity of WT and
146 Δ*esxC* membranes. Compared to the WT, the cytosolic membrane of the Δ*esxC* mutant showed
147 a mild but statistically significant increase in rigidity (Fig. 2 A). Furthermore, we stained WT and
148 with a fluorescent membrane dye DiI12C, which has been used detect regions of increased fluidity
149 in bacteria[25]. As reported previously for *S. aureus*, we observe a few fluid regions in the WT, and
150 an uneven staining of the membrane. In contrast, a very weak staining of the membranes was
151 observed for the Δ*esxC* mutant (Fig. 2 B), which may indicate a decrease in membrane fluidity.
152 Finally, membrane fluidity was measured using the fluorescent dye Laurdan (6-dodecanoyl-2-
153 dimethylaminonaphthalene) which is incorporated into the membrane bilayer[26]. Logarithmic phase
154 WT cells treated with Laurdan showed a lower average generalized polarisation value of 0.33
155 compared to 0.42 for *ΔesxC* suggesting that the membrane of the mutant is more rigid in
156 comparison to that of the WT (Fig. 2 C).

157 Overall, the data indicate that EsxC contributes to *S. aureus* cell surface structure through
158 modulating membrane fluidity.
159
160 **T7SS mutants have altered protein localization and membrane protein profiles**
161 Functional membrane microdomains (FMMs) act as scaffolds for protein interactions and
162 oligomerization[27]. Bacterial flotillins are key scaffolding proteins which have been shown to
163 regulate membrane fluidity and protein organisation[28]. FloA also interacts with structural T7SS
164 proteins EssA and EssB, however interactions with effector proteins were not investigated[12]. To
165 investigate possible protein localisation defects in the T7SS mutants, the distribution of the
166 staphylococcal flotillin FloA was examined.
167
168 When exponentially growing FloA-eYFP expressing WT and Δ*esxC* and Δ*essC* mutants were
169 studied by fluorescence microscopy, a different localisation of GFP-tagged flotillin was observed
170 in the Δ*esxC* and Δ*essC* mutants compared to the WT (Fig. 2 D). The WT appears to display a
171 more homogenous distribution of flotillin throughout the membrane while both T7SS mutants have
172 a more defined heterogenous punctate distribution. The number of FloA foci per cell were
173 quantified. The WT had a broader distribution of with generally higher numbers of foci, but smaller
174 and with lower levels of fluorescence, while mutants had fewer foci but with higher levels of
175 fluorescence. This suggests that the T7SS components may have a role in modulating flotillin
176 localisation.
177
178 Previously, we reported that the mutants Δ*esxC* and Δ*essC* had distinct total protein profiles with
179 and without treatment with linoleic acid[20]. Given the changes seen in bacterial membranes in the
180 absence of T7SS proteins, we examined global changes in the protein content in the membrane.
181 Membrane fractions extracted from logarithmic phase (OD_{600} 3.0) cultures of WT, Δ*esxC* and
182 Δ*essC* were analysed by LC/MS. 13 and 15 proteins were altered in abundance [log2 (fold

183 change) = 1.0, $P < 0.05$] in Δ*esxC* and Δ*essC* respectively in relation to the WT. While 6
184 differentially abundant proteins were common to both mutants, overall, both mutants displayed
185 distinct profiles (Table 1). Interestingly, EssD, a T7SS substrate which is a nuclease, is decreased
186 significantly in the membranes of Δ*esxC* but not in Δ*essC.* To study the impact of EssC and EsxC
187 on protein export, a secretome analysis from culture supernatants was performed. Secretome
188 analysis showed a lower abundance of EssD in Δ*esxC* compared to WT (Table S1). In agreement
189 with the requirement of transporter EssC for T7 secretion, EssD, and other T7SS proteins (EsxA
190 and EsxC) were depleted in the secretome of Δ*essC* (Table S1). Again, there was some overlap
191 in the proteins secreted by both T7SS mutants, although many proteins were distinct to either
192 mutant strain.
193 Thus, the T7SS mutants show distinct changes to the overall membrane protein profiles, along
194 with changes in localisation of specific proteins.
195
196 **T7SS mutants display altered cell surface morphology**
197 To examine the cell surface of T7SS mutants we visualised the WT, Δ*esxC* and Δ*essC* using
198 scanning electron microscopy. The cell surface of WT grown to early logarithmic phase have the
199 typical smooth spherical shape of *S. aureus*, however, the isogenic mutants Δ*esxC* and Δ*essC*
200 appear deflated with dents or hollows (Fig. 3 A). The WT phenotype was restored in Δ*esxC*
201 complemented with a plasmid expressing *esxC* (Fig. 3 B). Interestingly, this cell surface defect is
202 not seen in all T7SS mutants as strains lacking EsxD (Δ*esxD*) does not have a defective cell
203 surface phenotype (Fig. 3 A). *S. aureus* cell surface alterations were seen in strains USA300 (LAC)
204 and Newman lacking EsxA (*ΔesxA)*, but not in *ΔesxB* (Fig. S4). However, RN6390 strains lacking
205 *esxC* and *essC* showed very little surface defects (Fig. S4). Differences seen in surface
206 morphologies between WT and mutants were not due to growth rate differences, as growth rates
207 of all mutant strains in the different strain backgrounds (*ΔessC*, *ΔesxC*, *ΔesxA*, Δ*esxB,* and
208 *ΔesxD)* in TSB, were similar to that of their WT (Fig. S1). Our data suggest that the cell envelopes

209 of mutants lacking specific T7SS components were altered, potentially due to a defect in the cell
210 membrane and/or cell wall structure.
211
212 **T7SS mutants show decreased rate of cell wall synthesis**
213 To investigate if the surface structure changes were associated with a defect in cell wall structure
214 or synthesis, transmission electron microscopy was undertaken to investigate any differences
215 between the cell wall ultrastructure of the T7SS mutants. However, there were no clear differences
216 in cell wall diameters between strains (Fig. S5). To study whether peptidoglycan synthesis and
217 accumulation were affected in the T7SS mutants, HADA, a fluorescent D-amino acid was used[29].
218 The dye was either added to a fresh subculture and grown until the bacteria reached logarithmic
219 phase or added for 10 min once the culture reached an OD_{600} of 1. No differences were observed
220 in the cells which had been grown with TSB supplemented with HADA (Fig. 4 A, B), however
221 addition of HADA during exponential phase growth revealed a faster accumulation of HADA in the
222 WT compared to *ΔessC* and *ΔesxC* (Fig. 4 A, C). This suggests that T7SS mutants displayed a
223 decreased rate of new peptidoglycan synthesis.
224
225 ***ΔesxC* and *ΔesxA* have a more negative cell surface charge**
226 As we observe cell surface defects and changes to peptidoglycan synthesis, we next tested if the
227 disruption of the T7SS could alter other cell surface properties like surface charge. A cytochrome
228 binding assay was employed to measure surface charge; the binding of cytochrome C, a highly
229 positively charged protein, is directly proportional to the net negative surface charge of *S. aureus*
230 cells[30]. A significantly higher level of binding of cytochrome to cell surface of Δ*esxC* and Δ*esxA*
231 was observed compared to the USA300 WT strains, JE2 and LAC respectively. However, there
232 was no difference in the levels of binding between the WTJE2 and Δ*essC* (Fig. 5 A, C). This
233 suggests that the cell surface of Δ*esxC* is overall more negative. Much lower levels of cytochrome
234 C bound to USA300 LAC WT and Δ*esxB* suggesting these cell surfaces are also less negative

235 (Fig. 5 C). Colony forming unit (CFU) counts from samples after cytochrome C addition showed
236 no differences in cell numbers and therefore it is unlikely that bacterial cell numbers influenced
237 cytochrome C binding (Fig.5 B, D). These data indicate that the T7SS effectors affect the surface
238 charge of *S. aureus*.
239
240 **Δ*esxC* shows increased binding of daptomycin**
241 *S. aureus* has been reported to resist daptomycin through possessing a more positive surface
242 charge, causing electrostatic repulsion of the positively charged daptomycin calcium complex, and
243 thus preventing binding[31,32]. Based on the increased negative surface charge observed for the
244 T7SS mutants in the cytochrome C assay, we hypothesised that daptomycin could bind more
245 easily in the absence of a functional T7SS. To test this, daptomycin was tagged with BODIPY and
246 used to quantify binding via fluorometry and to visualise bound daptomycin by fluorescence
247 microscopy. In the presence of daptomycin, a higher level of daptomycin seen to bind around the
248 septum for the WT (Fig. 5 E, F) as reported previously[33]. The *ΔesxC* mutant showed significantly
249 higher fluorescence in comparison to the WT. Thus, our data suggest that the increased
250 daptomycin binding may be due to reduced electrostatic repulsion of daptomycin by *ΔesxC*.
251
252 When we stained bacteria with propidium iodide (PI), a fluorescent intercalating agent which
253 cannot pass through the membranes of viable cells, cytosols of daptomycin-treated Δ*esxC* and
254 Δ*essC* showed a higher intensity of PI compared to the WT as quantified by fluorescence
255 microscopy (Fig. 6 A, B). We also stained cells with the lipid staining dye FM1-43. FM1-43 staining
256 was of similar intensity, although it appears less ordered in the daptomycin-treated Δ*esxC* and
257 Δ*essC* samples (Fig. 6 A, B). Thus, membranes of the Δ*esxC* and Δ*essC* mutants are more
258 permeable in presence of daptomycin.
259
260 **Decreased survival of T7SS mutants during intracellular infection with daptomycin**

261 *S. aureus* is a facultative intracellular pathogen, and daptomycin is considered to kill intracellular
262 bacteria effectively. Hence, we wanted to determine if deletion of *essC* and *esxC* from *S. aureus*
263 would enhance intracellular killing activity. A549 human lung epithelial cells[15] infected with *S.*
264 *aureus* were treated with a high concentration of daptomycin (20 µg/ml). While there were no
265 differences in the bacterial numbers between the WT and T7SS mutants in internalised bacteria
266 (1 h after infection), a significant decrease was observed in the numbers of Δ*esxC* and Δ*essC*
267 surviving within cells treated with daptomycin in comparison to WT after 4 h and 24 h after infection
268 (Fig. 7 A). Notably, there was a significant number of WT *S. aureus* bacteria surviving intracellularly
269 after treatment with daptomycin. Confocal microscopy imaging of infected cells also showed
270 similar number of bacterial cells entering the mammalian cells but more *S. aureus* WT remaining
271 compared to *ΔessC* and *ΔesxC* 24 h after infection in presence of daptomycin (Fig. 7 B, C).
272 USA300 JE2 WT, *ΔessC* and *ΔesxC* showed no differences in growth rate in the cell culture
273 medium, DMEM-10, indicating that the differences seen in the infection assay were not due to the
274 ability of the mutants to grow differently (Fig. S6A); as with the TSB, a growth defect was seen in
275 the T7SS mutants in presence of daptomycin (Fig. S6B). Therefore, our data suggest that
276 daptomycin is more effective in killing intracellular *S. aureus* in the absence of T7SS.
277
278 **T7SS mutants are more sensitive to daptomycin in a skin infection model**
279 We next investigated how effective daptomycin was in curbing *S. aureus* infection *in vivo* and if
280 the absence of T7SS had any impact on daptomycin killing *in vivo*. T7SS proteins have been
281 reported to be important in various murine infection models[6,8,34]. Here, we employed a localised
282 murine skin abscess model to investigate both the role of T7SS protein EsxC during skin infection
283 and if its presence could affect daptomycin activity.
284 7-8-week-old BALB/c mice were infected with *S. aureus* WT and *ΔesxC* intradermally, followed by
285 treatment (intravenous) 2 h post infection (h.p.i) and every 24 h after, with 10 mg/kg daptomycin.
286 Bacterial counts were obtained from skin tissue 24 or 72 h.p.i. Weight and skin lesion diameters

287 were recorded every day. In the groups not treated with daptomycin, bacterial counts from the site
288 of infection (lesions) showed no significant difference between WT and *ΔesxC* infected mice after
289 24 or 72 h of infection. A significant decrease was seen in the numbers of *ΔesxC* present in the
290 skin of daptomycin-treated mice compared to the untreated group 24 and 72 h.p.i, while this was
291 not the case for the WT infected group. The daptomycin treated *ΔesxC* infected group had lower
292 mean bacterial count (7.32×10^7 at 24 h and 7.39×10^6 at 72 h) than the WT-infected, daptomycin
293 treated group (1.12×10^8 at 24 h and 1.45×10^7 at 72 h) and (Fig. 8A and B). No significant
294 differences were observed between the areas of lesions measured for WT or *ΔesxC* after 24 h or
295 72 h infections and in daptomycin-treated mice (Fig S7). Although the dose of daptomycin used in
296 the time frame of treatment was not sufficient to treat WT infection, this data suggests that the
297 strain lacking EsxC was more susceptible to daptomycin *in vivo*. Interestingly, when cytokines
298 TNF-α and IL-β were measured, there was a significant difference between the treated and
299 untreated groups for both strains 72 h.p.i. (Fig 8 C and D). The mutant induced significantly less
300 IL1-β than the WT at 72 h.p.i., irrespective of daptomycin treatment (Fig 8 D).
301
302 **Discussion**
303 The *S. aureus* T7SS has been strongly associated with staphylococcal virulence and ability of this
304 pathogen to persist during infection[7]. Its importance for bacterial competition between *S. aureus*
305 strains has been recently highlighted[13]. However, the role of this system in staphylococcal
306 physiology has been poorly defined. Here we report that the T7SS is critical in maintaining cell
307 membrane homeostasis through modulating membrane properties including fluidity, accompanied
308 by changes in membrane protein localisation, changes to the rate of cell wall synthesis and surface
309 charge. Consequently, T7SS impacts activity of membrane acting drugs including daptomycin, a
310 key drug used to treat resilient staphylococcal infections. Our data demonstrate that T7SS can
311 modulate the activity of daptomycin both intracellularly as well as during infection *in vivo*.
312

313 Several studies in mycobacterial species have linked the T7SS to cell surface integrity in different
314 ways[19,35-38]. The ESX-1 system has been previously reported to impact cell membrane
315 permeability in *M. tuberculosis*, although this effect appeared to be strain specific [35]. However,
316 ESX-5 which is considered essential for *in vitro* growth, has been linked to mycobacterial capsular,
317 cell wall and outer membrane permeability[19,36,39]. As ESX-5 was no longer essential in *M. marinum*
318 when the membrane was permeabilised, it was proposed that ESX-5 mediates transport of cell
319 envelope proteins to the outer membrane required for uptake of essential nutrients. While these
320 substrates have not been identified, a substrate PPE-10 was associated with capsular
321 integrity[19,36]. In *S. aureus,* we previously reported that the effectors, EsxC, and the ATPase, EssC,
322 were associated with maintenance of membrane integrity in response to antimicrobial host fatty
323 acids[20].
324
325 T7SS proteins have previously been linked with membrane fluidity and flotillins. Higher levels of
326 T7SS transcription were associated with a decrease in membrane fluidity, caused by the fatty acid
327 kinase complex, which incorporates host fatty acids into the membrane, inducing a change in
328 membrane dynamics[24]. *S. aureus* encodes one flotillin homolog, which shares 84% homology with
329 the FloA protein in *B. subtilis* [40]. FloA (also referred to as FloT) in *S. aureus,* has been linked to
330 T7SS assembly [12]. T7SS membrane proteins interact with FloA within functional membrane
331 microdomains (FMM) promoting more efficient interactions between T7SS membrane
332 components EssB and EssA, helping incorporate EssA into the EssC-EsaA-EssB pre-complex.
333 Here we see that the membrane of the *ΔesxC* mutant was more rigid than the WT, and floA
334 appears to localize differently in the membranes of this mutant. It is not clear whether the
335 localisation of the flotillin is due to the more rigid membrane in the mutants or if the flotillin
336 mislocalisation in the mutants causes the membrane to become more rigid, as flotillins have a role
337 in spatially organising membrane domains by acting as scaffolds to guide proteins to the correct
338 membrane areas [28]. Thus, EsxC may have a direct but transient interaction with FloA in the FMM

339 or an indirect impact upon other membrane-associated proteins which could impact the lipid
340 packing and fluidity of the membrane.
341
342 While we demonstrate that T7SS and specific substrates play a role in maintaining membrane
343 integrity, we do not know how the T7SS contributes to this. There are multiple possibilities 1.
344 substrates like EsxC are chaperones for membrane proteins and play a role in targeting them to
345 the membrane. A recent bacterial two-hybrid library screening we performed was not successful
346 in identifying any direct bacterial interactors, however it is possible that such interactions are
347 transient. 2. T7SS proteins may impact the state of the membrane by binding other molecules like
348 metal ions required for maintaining stability of the membrane. 3. destabilizing this complex
349 secretion apparatus has a non-specific effect on the physical structure of the membrane.
350
351 It is interesting that not all T7SS proteins/ substrates have a cell surface associated defect. This
352 indicates that only certain substrates of the system are mediating this effect. EsxD and EsxB did
353 not appear to be associated with surface morphology defects as observed for EsxC and EsxA.
354 Surface charges corelated well with daptomycin sensitivity indicating that these substrates did not
355 play a role in the membrane homeostasis. Surface charge measurements of WT and mutants
356 using a cytochrome C binding assay revealed that Δ*esxC* and Δ*esxA* had an increased negative
357 surface charge, whereas *ΔesxB* and *ΔessC* did not display any differences in charge to the WT.
358 This may be because esxC is still produced by *ΔessC*, although it is not secreted, thus
359 accumulating in the cytosol and membrane, further indicating that EsxC plays a key role in
360 maintaining surface charge.
361
362 While EsxA is conserved across all *S. aureus* strains, only the essC1 locus encodes EsxC [8,9]. It is
363 however likely that all *S. aureus* strains encode a protein orthologous to EsxC as proteins in
364 module 2, with variants essC2 – 4, have not yet been characterised. Therefore, it is possible that

365 one of the hypothetical proteins has functions like EsxC. Additionally, several of the phenotypes
366 reported for strains lacking EsxC were also seen in strains which lacked EsxA. Previous reports
367 have suggested that EsxC and EsxA interact[11]. Therefore, this could mean that interactions
368 between EsxC and EsxA may be important in modulating membrane integrity.
369
370 Daptomycin is thought to bind to the cell membrane before forming a complex with cell wall
371 biosynthesis machinery, preventing cell wall synthesis, before dispersing throughout the bacterial
372 membrane causing depolarisation[41]. Daptomycin, although not a cationic antimicrobial peptide,
373 forms a highly positively charged complex with calcium to become active. Significantly more
374 daptomycin was bound to the *ΔesxC* than the WT, which supports the hypothesis that the
375 decrease in surface charge measured in *ΔesxC* allows easier binding of daptomycin to the cell
376 membrane. However, the surface charge of *ΔessC* does not differ from the WT and therefore
377 increased susceptibility to the positively charged daptomycin is likely not caused solely by charge-
378 dependent binding. Also, in contrast to daptomycin, membrane targeting antimicrobials bithionol
379 and gramicidin are uncharged[23,42], therefore surface charge and thus decreased electrostatic
380 repulsion of the antibiotic in the T7SS mutants is not the only factor involved in increased
381 sensitivity. Daptomycin appears to have the highest impact on the T7SS mutants whereas
382 bithionol appears to have the lowest activity. As all three antimicrobials have different mechanisms
383 of action once bound to the membrane before causing membrane depolarization, the subsequent
384 steps after membrane binding appear to be important for efficacy. Therefore, perhaps daptomycin
385 treatment which impacts both the cell membrane, and the cell wall causes a larger effect in the
386 T7SS mutants.
387
388 While daptomycin increases killing of T7SS mutants *in vivo*, at the dose and strain of *S. aureus*
389 used, there was no impact of the T7SS in bacterial survival during acute skin infection. T7SS
390 proteins have been previously reported to be important for bacterial virulence using invasive

391 kidney abscess, nasal colonisation and skin infection models, although studies have used different
392 *S. aureus* strains[6,8,34]. The lack of decrease in the lesion size of the T7SS mutant-infected mice
393 treated with daptomycin, unlike the trend towards decreased lesion size observed for the WT (Fig
394 S7), could indicate that the increased killing of bacteria may cause an altered local immune
395 response. This is supported by the different levels of inflammatory cytokines seen in the
396 daptomycin treated WT and the mutant-infected mice. While our infection studies indicate a
397 potential role for EsxC (in a USA300 strain background) in modulation of IL1-β, the data indicate
398 that it may not play a role in bacterial survival during skin infection. A recent study reported that in
399 a *S. aureus* strain WU1, the T7SS was important only for invasive infection and not localized nasal
400 colonization [43].
401
402 Currently, levels of resistance to daptomycin are low, however, with increasing resistance in other
403 last line antibiotics, such as vancomycin, the use of daptomycin going forward will increase[44]. The
404 increased use of daptomycin will likely lead to the occurrence of more resistant isolates, therefore
405 research into new antibiotics, and targeting new proteins that can enhance existing treatments
406 could be a powerful approach. Our data indicate that inhibitors of T7SS proteins or of T7SS
407 secretion could have excellent potential in combination drug therapies.
408
409 **Materials and Methods**
410 **Resource availability**
411 **Lead contact**
412 Further information and requests for resources and reagents should be directed to and will be
413 fulfilled by the lead contact, m.unnikrishnan@warwick.ac.uk

414 **Materials availability**

415 This study did not generate new unique reagents.
416

417 **Experimental model and study participant details**

418 **Animals**

419 All animal procedures were carried out as per protocols in the Project Licence PCEC27E7D. All
420 local ethical and home office approvals were obtained for animal experimentation. For the murine
421 skin abscess model, female 7/8-week-old BALB/c mice (Charles River Laboratories, UK) flanks
422 were shaved before injection, and inoculated through an intradermal route with 50 µl of bacterial
423 suspension per flank (one injection on each flank), resulting in a final bacterial count of 1-2 x 10^6
424 per mouse. Overnight *S. aureus* cultures were subcultured, grown to OD_{600} of 1, centrifuged and
425 washed twice with PBS, and diluted in PBS to achieve a final CFU/ml of 1-2 x 10^7 for infection. 2
426 h after infection mice were given an intravenous dose of daptomycin or PBS via tail vein injection.
427 This was repeated once every 24 h. During the experiment, mice were weighed daily, and any
428 abscess formation was measured and recorded. After 24 h or 72 h mice were euthanised by CO_2
429 inhalation and skin at the infection site was incised. The skin samples were weighed and
430 homogenised in PBS using a FastPrep (MP Biomedicals), at 4 m/s for 60 seconds for a total of 6
431 cycles. Homogenates were diluted in PBS and CFU counts were determined and normalized to
432 tissue weight.
433

434 **Method details**

435 **Bacterial strains**

436 *S. aureus* strains used in this study are included in Table 2. Strains were cultured aerobically in
437 tryptic soy broth (TSB) (Sigma-Aldrich) at 37°C with aeration at 180 rpm overnight. Overnight
438 cultures were subcultured into fresh TSB and grown to a density of optical density (OD_{600}) of 1,
439 unless stated otherwise. For complemented strains TSB was supplemented with 10 µg/ml
440 chloramphenicol.

441 **Growth curves**

442 Overnight bacterial cultures were diluted to an OD_{600} of 0.1 in TSB or TSB supplemented with
443 antimicrobials where specified. Bacteria were grown in a 96-well plate with shaking and the OD_{600}
444 was measured every 15 min with a FLUOstar OMEGA plate reader (BMG Labtech, UK). At
445 appropriate time points 100 µl of the samples were taken for CFU determination.

446 **Daptomycin killing assay**

447 Bacterial cultures were grown overnight in TSB, diluted to an OD_{600} of 0.15 and grown to log
448 phase. Bacterial cultures were then treated with 10 µg/ml of daptomycin (Acros Organics) in the
449 presence of 1 mM $CaCl_2$ (Fisher Scientific) and incubated at 37ºC for a further 2 h. Aliquots were
450 removed at indicated timepoints, serially diluted in PBS and plated on tryptic soy agar (TSA) for
451 CFU determination.

452 **Scanning Electron Microscopy**

453 Overnight bacterial cultures were diluted to an OD_{600} of 0.15 and grown to an OD_{600} of 1 in TSB.
454 The pellet was washed with PBS twice before dropping onto poly-lysine coated 12 mm circular
455 coverslips. Samples were fixed with 2.5% glutaraldehyde in PBS for 1 h at 4°C. The bacterial cells
456 were dehydrated by washing with a series of ethanol solutions (20%, 50%, 70%, 90% and 100%)
457 and dried with hexamethyldisilazane. The samples were sputter coated with carbon and then
458 observed using a Gemini SEM 500 (Zeiss).

459 **Transmission Electron Microscopy**

460 Overnight bacterial cultures were diluted to an OD_{600} of 0.15 and grown to an OD_{600} of 1 in TSB.
461 The pellet was washed in PBS three times and fixed with paraformaldehyde and glutaraldehyde
462 for 1 h at room temperature (RT). Pellets were rinsed a further three times in PBS before
463 incubation with 1% osmium tetroxide for 1 h at RT. The bacterial cells were dehydrated by washing
464 with a graded acetone series for 20 min each and transferred to graded acetone epoxy resin
465 mixture for 45 min each. Cells were incubated in pure resin for 24 h before being hardened
466 overnight at 60°C. The specimens were sectioned into 90 nm slices using an ultramicrotome

467 (RMC) before being placed onto grids and stained with heavy metals. The samples were
468 visualised using a TEM-2100Plus (Jeol).

469 **Determination of membrane fluidity by Laurdan staining**

470 Membrane fluidity was measured using the fluorescent dye Laurdan (Sigma). Logarithmic phase
471 *S. aureus* was grown, and 1 ml aliquots were washed in PBS. The samples were incubated with
472 a final concentration of 100 µM Laurdan for 5 min at RT in the dark. Samples were washed four
473 times in PBS and 200 µl was transferred to a black walled 96 well plate in triplicate. Membrane
474 fluidity was determined by using an excitation wavelength of 350 nm and measuring fluorescence
475 at 460 nm and 500 nm emission wavelengths on a BioTek Cytation 5 Cell Imaging Multimode
476 Reader (Agilent). The generalised polarisation (GP) value was calculated using the following
477 calculation, $GP = (I_{460}-I_{500}) / (I_{460}+I_{500})$.

478 **DiIC12 staining**

479 O/N bacterial cultures were diluted to an OD600 of 0.15 in TSB with 1 µg/mL 1,1′-didodecyl-
480 3,3,3′,3′-tetramethylindocarbocyanine perchlorate (DiIC12) (Invitrogen). Cultures were grown to
481 an OD600 of 1.0, centrifuged and washed twice with fresh TSB. Samples were spotted on to
482 agarose pads and imaged using a Leica DMi8 widefield microscope (Leica Microsystems, UK).
483 Acquired images were analysed with the ImageJ processing package, Fiji.

484 **Cytochrome C binding assay**

485 Overnight bacterial cultures were pelleted and washed with 20 mM MOPS buffer, pH 7. The cells
486 were resuspended in MOPS buffer at an OD_{600} of 1 and incubated with 50 µg/ml cytochrome C at
487 RT for 15 min. The cells were pelleted and the remaining cytochrome C in the supernatant was
488 measured spectrophotometrically at OD_{410} using a FLUOstar OMEGA plate reader (BMG Labtech,
489 UK).

490 **HADA incorporation assay**

491 Peptidoglycan synthesis was investigated by incorporation of HCC-amino-D-alanine (HADA)
492 incorporation. Overnight *S. aureus* cultures were diluted into TSB supplemented with 25 µM HADA

493 and incubated at 37ºC in the dark. When OD_{600} of 1.0 was reached cultures were washed three
494 times and fixed with 4% PFA. Alternatively, cultures were treated with daptomycin for 30 min before
495 washing and fixing. Microscopy was undertaken on these samples using the DAPI filter set on a
496 Leica DMi8 widefield microscope.

497 **Localisation of FloA-eYFP**

498 An overnight culture was diluted and grown to logarithmic phase. 1 ml of culture was centrifuged
499 and washed with PBS before fixing with 4% PFA at RT for 15 min. The bacteria were pelleted and
500 washed twice in PBS before resuspension in 100 µl of PBS. Bacteria were imaged using API
501 Deltavision 2 (Applied Precision Instruments) widefield microscope using YFP filter set at 100x
502 magnification.

503 **Synthesis of Daptomycin BODIPY**

504 A 1 mg/ml stock solution of 1-ethyl-3-(3-dimethylaminopropyl) carbodiimide hydrochloride (EDC),
505 N-Hydroxysuccinimide (NHS), daptomycin and BODIPY was prepared in DMSO. Th mixture was
506 stirred for 16-24 h at RT. 10 µl of the crude sample was removed and diluted with High
507 Performance Liquid Chromatography (HPLC) solvent, filtered and used for HPLC analysis. The
508 solution was purified by dialysis with ultrapure water to remove EDC, NHS and any other unwanted
509 by-products with a membrane cut-off of 100 – 500 Da. The water was replaced every 2 h for a
510 total of 2 times. The sample was freeze dried to remove the water.

511 **Daptomycin BODIPY binding**

512 *S. aureus* was grown as previously described and treated with daptomycin once logarithmic phase
513 had been reached. The samples were incubated at 37ºC for 30 min in the dark then washed with
514 PBS three times. 200 µl were aliquoted into black 96 well plates in triplicate and fluorescence was
515 measured using a BioTek Cytation 5 Cell Imaging Multimode Reader (Agilent). The excitation
516 wavelength used was 488 nm and emission wavelength used was 530 nm.

517 **Propidium Iodide Staining**

518 Bacterial cultures were grown in TSB to an OD_{600} of 1, centrifuged and resuspended in TSB
519 supplemented with 1 mM $CaCl_2$. Samples with and without daptomycin were incubated at 37°C
520 for a further hour before propidium iodide and FM1-43 were added to a final concentration of 3 µM
521 and 10 ng/µl, respectively. Samples were washed in PBS twice and spotted onto agarose pads.
522 Once dry, cover slips were mounted using DAPI anti-fade mounting fluid. Samples were imaged
523 on a Leica DMi8 widefield microscope (Leica Microsystems, UK) using 100x objective. Propidium
524 iodide, FM1-43 and DAPI were imaged using the Texas Red, FITC and DAPI filter sets
525 respectively.

526 **Invasion and survival Assay**

527 Infection assays were carried out in 24-well tissue culture treated plates (Falcon), or RS treated
528 glass chamber slides (154526, Nunc, Lab Tek II). Overnight *S. aureus* cultures were diluted to an
529 OD_{600} of 0.15 and grown to an OD_{600} of 1. Cultures were resuspended in DMEM media to a density
530 of 2.5 x10^6 colony forming units (CFU)/ml. A549 epithelial cells were seeded in 24 well plates at a
531 density of 2.5 x 10^5 a day before being infected with *S. aureus* at a multiplicity of infection (MOI)
532 of 10. Cells were infected for 1 h at 37°C with 5% CO_2. To kill any extracellular bacteria, cells were
533 washed with DMEM media containing 20 µg/ml lysostaphin (Sigma-Aldrich) and 50 µg/ml
534 gentamycin (Melford) and incubated for a further 30 min. Cells were washed twice with PBS, lysed
535 with 1 ml cold sterile water and vigorous pipetting before plating for CFU determination. To
536 investigate the course of infection after extracellular bacterial killing, the cells are washed twice
537 with PBS and refreshed with DMEM with 1 mM $CaCl_2$ only or DMEM supplemented with 1 mM
538 $CaCl_2$ and 10 µg/ml daptomycin and incubated until the desired timepoint. The above protocol to
539 lyse the cells is then followed.

540 **Confocal microscopy**

541 At required timepoints A549 cells infected with *S. aureus* were washed twice with PBS and fixed
542 with 4% paraformaldehyde (PFA) for 15 min. The chamber slide wells were washed in 1 ml PBS
543 and permeabilised with 1% saponin, 0.1% triton X-100 in PBS for 20 min at RT. Cells were blocked

544 with 3% BSA in PBS for 30 min at RT. Slides were then washed with 1% BSA in PBS and twice
545 with PBS only. Cells were stained with phalloidin 650 in 1% BSA for 40 min at RT and vancomycin-
546 BODIPY in 1% BSA for 20 min. DAPI anti-fade mounting fluid was added to the slide. Samples
547 were imaged using a spinning disk confocal UltraVIEW (PerkinElmer).

548 **Preparation of samples for proteomics**

549 **Preparation of membrane fractions:** *S. aureus* strains were grown to an OD_{600} of 3.0 in TSB.
550 After centrifugation of cultures, pellets were washed with PBS and resuspended PBS
551 supplemented with one cOmplete™, Mini, EDTA-free Protease Inhibitor Cocktail tablet, 250 mM
552 sucrose, 1 mM EDTA, and 50 µg/mL lysostaphin. Samples were incubated for 15 min at 37ºC.
553 Samples were aliquoted into lysing matrix B tubes (MP Biomedicals™), and bacteria were lysed
554 with a Fastprep machine (6.5 m/s, 2 x 45 s). Samples were centrifuged at 11 000 × *g* for 15 min,
555 and supernatants were collected and then ultracentrifuged (230 000 × *g* for 30 min at 4ºC) in clean,
556 thick wall polyallomer tubes. Pellets were resuspended in 400 µL PBS supplemented with 250 mM
557 sucrose and 10% glycerol.

558 **Preparation of culture supernatant**: *S. aureus* strains were grown to an OD600 of 3 in TSB.
559 After centrifugation of cultures, supernatants were sterile-filtered and incubated at 4°C overnight
560 with 10% trichloroacetic acid and 50 µM sodium deoxycholate in presence of one cOmplete™,
561 Mini, EDTA-free Protease Inhibitor Cocktail tablet (Sigma-Aldrich, UK). The precipitated proteins
562 were centrifuged at 10 000 g at 4°C for 15 min, gently washed with acetone twice, dried at RT for
563 10 min and resuspended in PBS. After denaturation, precipitated proteins were run on a gel until
564 all the proteins had moved from the stacking gel into the resolving gel. The gel was then stained
565 with InstantBlueTM (Sigma-Aldrich, UK) for 3 h, after which the protein bands were excised and
566 diced. Proteins were in-gel digested with trypsin as described elsewhere[45]. Briefly, proteins were
567 reduced and alkylated for 5 min at 70°C with 10 mM TCEP [tris(2-carboxyethyl) phosphine] and

568 40 mM CAA (2-chloroacetamide), respectively. Tryptic digestion was carried out at O/N at 37°C
569 in 50 mM ABC.

570 **Label-free protein quantification.**

571 Peptides prepared for proteome analyses were desalted and concentrated with a C18 cartridge in
572 40 µL MS buffer (2% acetonitrile plus 0.1% trifluoroacetic acid). For each sample, 20 µL were
573 analysed by nanoLC-ESI-MS/MS using the Ultimate 3000/Orbitrap Fusion instrumentation
574 (Thermo Scientific), and a 90-minute LC separation on a 50 cm column. The data were used to
575 interrogate the Uniprot *Staphylococcus aureus* USA300 database UP000001939, and the
576 common contaminant database from MaxQuant (Cox et al., 2014). MaxQuant software was used
577 for protein identification and quantification using 567 default settings. Intensities were log2-
578 transformed with the Perseus software, and proteins with one or no valid value for every sample
579 in triplicate were filtered.

580 The proteomics data have been deposited to the ProteomeXchange Consortium via the PRIDE
581 partner repository with the dataset identifier PXD047096 and 10.6019/PXD047096. Membrane
582 proteomic and secretome samples are labelled MS18-178 and MS19-126, respectively.

583 **ELISA**

584 The levels of mouse TNF-α and IL-1β were quantified from the supernatant of homogenised skin
585 samples using Mouse TNF-alpha DuoSet ELISA (DY410) or Mouse IL-1 beta/IL-1F2 DuoSet
586 ELISA (DY401) (R&D Systems) following the manufacturer's protocols. The optical density was
587 measured at 540 nm and subtracted from readings at 450 nm using the BioTek Cytation 5 Cell
588 Imaging Multimode Reader (Agilent). Concentrations were calculated from standard curves run in
589 parallel.

590 **Image Analysis**

591 All microscopy images were analysed using FIJI (ImageJ, Version 2.0.0-rc-69/1.52p). To calculate
592 fluorescence, a threshold value was set, and area or number of bacterial cells was used to
593 normalise fluorescent values against.

594 **Statistical Analysis**

595 Statistical analysis was performed using GraphPad Prism 9.0 (MacOS version 9.5.1). Pairwise
596 statistical analysis was carried out by the Man-Whitney U test for two groups, and one or two-way
597 ANOVAs for multiple groups, followed by post-hoc Tukey's HSD tests where necessary.
598 Significance was denoted by asterisks; * = P < 0.05, ** = P < 0.01, *** = P < 0.001, **** = P <
599 0.0001 and ns = not significant. The fold changes and *P* values of the proteomics data were
600 calculated with the R package limma[46].

601

602 **Acknowledgements**

603 We would like to acknowledge funding from MIBTP (grant number) to Victoria Smith and the
604 Medical Research Council grant (MR/N010140/1) for funding.
605 We would like to thank Novartis Vaccines, Siena (GSK biologicals) Italy for providing the *ΔesxA*
606 and *ΔesxB* strains, and Prof Tracy Palmer for providing the RN6390 *ΔesxC* and *ΔessC* strains,
607 used in this study. We acknowledge the Midlands Regional Cryo-EM Facility, hosted at the
608 Warwick Advanced Bioimaging Research Technology Platform, for the use of the JEOL 2100Plus.

609

610 **Author contributions**

611 VS, AKT and MU conceptualised ideas, designed experiments, VS, GC, KEW, RGM, JY, AKT
612 conducted experiments, MU and SP provided resources for the study, VS, AKT, GC, KEW, RGM
613 and MU analysed data, AKT and MU supervised study, MU, VS and AKT drafted manuscript and
614 all authors were involved in reviewing manuscript draft.

615

616 **References**

617 1. Tong, S.Y., Davis, J.S., Eichenberger, E., Holland, T.L., and Fowler, V.G., Jr. (2015).
618 Staphylococcus aureus infections: epidemiology, pathophysiology, clinical manifestations,
619 and management. Clin Microbiol Rev *28*, 603-661. 10.1128/CMR.00134-14.

620 2. Chambers, H.F., and Deleo, F.R. (2009). Waves of resistance: Staphylococcus aureus in
621 the antibiotic era. Nature reviews. Microbiology *7*, 629-641. 10.1038/nrmicro2200.
622 3. Lee, B.Y., Singh, A., David, M.Z., Bartsch, S.M., Slayton, R.B., Huang, S.S., Zimmer, S.M.,
623 Potter, M.A., Macal, C.M., Lauderdale, D.S., et al. (2013). The economic burden of
624 community-associated methicillin-resistant Staphylococcus aureus (CA-MRSA). Clinical
625 microbiology and infection : the official publication of the European Society of Clinical
626 Microbiology and Infectious Diseases *19*, 528-536. 10.1111/j.1469-0691.2012.03914.x.
627 4. Cheung, G.Y.C., Bae, J.S., and Otto, M. (2021). Pathogenicity and virulence of
628 Staphylococcus aureus. Virulence *12*, 547-569. 10.1080/21505594.2021.1878688.
629 5. Bottai, D., Groschel, M.I., and Brosch, R. (2016). Type VII Secretion Systems in Gram-
630 Positive Bacteria. Curr Top Microbiol Immunol. 10.1007/82_2015_5015.
631 6. Burts, M.L., Williams, W.A., DeBord, K., and Missiakas, D.M. (2005). EsxA and EsxB are
632 secreted by an ESAT-6-like system that is required for the pathogenesis of Staphylococcus
633 aureus infections. Proceedings of the National Academy of Sciences of the United States
634 of America *102*, 1169-1174.
635 7. Unnikrishnan, M., Constantinidou, C., Palmer, T., and Pallen, M.J. (2017). The Enigmatic
636 Esx Proteins: Looking Beyond Mycobacteria. Trends in microbiology *25*, 192-204.
637 10.1016/j.tim.2016.11.004.
638 8. Kneuper, H., Cao, Z.P., Twomey, K.B., Zoltner, M., Jager, F., Cargill, J.S., Chalmers, J.,
639 van der Kooi-Pol, M.M., van Dijl, J.M., Ryan, R.P., et al. (2014). Heterogeneity in ess
640 transcriptional organization and variable contribution of the Ess/Type VII protein secretion
641 system to virulence across closely related Staphylocccus aureus strains. Molecular
642 microbiology *93*, 928-943. 10.1111/mmi.12707.
643 9. Warne, B., Harkins, C.P., Harris, S.R., Vatsiou, A., Stanley-Wall, N., Parkhill, J., Peacock,
644 S.J., Palmer, T., and Holden, M.T. (2016). The Ess/Type VII secretion system of

645 Staphylococcus aureus shows unexpected genetic diversity. BMC genomics *17*, 222.
646 10.1186/s12864-016-2426-7.
647 10. Bowman, L., and Palmer, T. (2021). The Type VII Secretion System of Staphylococcus.
648 Annu Rev Microbiol *75*, 471-494. 10.1146/annurev-micro-012721-123600.
649 11. Anderson, M., Aly, K.A., Chen, Y.H., and Missiakas, D. (2013). Secretion of atypical protein
650 substrates by the ESAT-6 secretion system of Staphylococcus aureus. Molecular
651 microbiology *90*, 734-743. 10.1111/mmi.12395.
652 12. Mielich-Suss, B., Wagner, R.M., Mietrach, N., Hertlein, T., Marincola, G., Ohlsen, K.,
653 Geibel, S., and Lopez, D. (2017). Flotillin scaffold activity contributes to type VII secretion
654 system assembly in Staphylococcus aureus. PLoS pathogens *13*, e1006728.
655 10.1371/journal.ppat.1006728.
656 13. Cao, Z., Casabona, M.G., Kneuper, H., Chalmers, J.D., and Palmer, T. (2016). The type
657 VII secretion system of Staphylococcus aureus secretes a nuclease toxin that targets
658 competitor bacteria. Nat Microbiol *2*, 16183. 10.1038/nmicrobiol.2016.183.
659 14. Ulhuq, F.R., Gomes, M.C., Duggan, G.M., Guo, M., Mendonca, C., Buchanan, G.,
660 Chalmers, J.D., Cao, Z., Kneuper, H., Murdoch, S., et al. (2020). A membrane-depolarizing
661 toxin substrate of the Staphylococcus aureus type VII secretion system mediates
662 intraspecies competition. Proceedings of the National Academy of Sciences of the United
663 States of America *117*, 20836-20847. 10.1073/pnas.2006110117.
664 15. Korea, C.G., Balsamo, G., Pezzicoli, A., Merakou, C., Tavarini, S., Bagnoli, F., Serruto, D.,
665 and Unnikrishnan, M. (2014). Staphylococcal Esx proteins modulate apoptosis and release
666 of intracellular Staphylococcus aureus during infection in epithelial cells. Infection and
667 immunity *82*, 4144-4153. 10.1128/IAI.01576-14.
668 16. Anderson, M., Ohr, R.J., Aly, K.A., Nocadello, S., Kim, H.K., Schneewind, C.E.,
669 Schneewind, O., and Missiakas, D. (2017). EssE Promotes Staphylococcus aureus ESS-

670 Dependent Protein Secretion To Modify Host Immune Responses during Infection. Journal
671 of bacteriology *199*. 10.1128/JB.00527-16.
672 17. Fyans, J.K., Bignell, D., Loria, R., Toth, I., and Palmer, T. (2013). The ESX/type VII
673 secretion system modulates development, but not virulence, of the plant pathogen
674 Streptomyces scabies. Molecular plant pathology *14*, 119-130. 10.1111/j.1364-
675 3703.2012.00835.x.
676 18. Flint, J.L., Kowalski, J.C., Karnati, P.K., and Derbyshire, K.M. (2004). The RD1 virulence
677 locus of Mycobacterium tuberculosis regulates DNA transfer in Mycobacterium smegmatis.
678 Proceedings of the National Academy of Sciences of the United States of America *101*,
679 12598-12603. 10.1073/pnas.0404892101.
680 19. Ates, L.S., Ummels, R., Commandeur, S., van de Weerd, R., Sparrius, M., Weerdenburg,
681 E., Alber, M., Kalscheuer, R., Piersma, S.R., Abdallah, A.M., et al. (2015). Essential Role
682 of the ESX-5 Secretion System in Outer Membrane Permeability of Pathogenic
683 Mycobacteria. PLoS genetics *11*, e1005190. 10.1371/journal.pgen.1005190.
684 20. Kengmo Tchoupa, A., Watkins, K.E., Jones, R.A., Kuroki, A., Alam, M.T., Perrier, S., Chen,
685 Y., and Unnikrishnan, M. (2020). The type VII secretion system protects Staphylococcus
686 aureus against antimicrobial host fatty acids. Sci Rep *10*, 14838. 10.1038/s41598-020-
687 71653-z.
688 21. Huang, H.W. (2020). DAPTOMYCIN, its membrane-active mechanism vs. that of other
689 antimicrobial peptides. Biochim Biophys Acta Biomembr *1862*, 183395.
690 10.1016/j.bbamem.2020.183395.
691 22. David, J.M., and Rajasekaran, A.K. (2015). Gramicidin A: A New Mission for an Old
692 Antibiotic. J Kidney Cancer VHL *2*, 15-24. 10.15586/jkcvhl.2015.21.
693 23. Kim, W., Zou, G., Hari, T.P.A., Wilt, I.K., Zhu, W., Galle, N., Faizi, H.A., Hendricks, G.L.,
694 Tori, K., Pan, W., et al. (2019). A selective membrane-targeting repurposed antibiotic with
695 activity against persistent methicillin-resistant Staphylococcus aureus. Proceedings of the

696 National Academy of Sciences of the United States of America *116*, 16529-16534.
697 10.1073/pnas.1904700116.
698 24. Lopez, M.S., Tan, I.S., Yan, D., Kang, J., McCreary, M., Modrusan, Z., Austin, C.D., Xu, M.,
699 and Brown, E.J. (2017). Host-derived fatty acids activate type VII secretion in
700 Staphylococcus aureus. Proceedings of the National Academy of Sciences of the United
701 States of America *114*, 11223-11228. 10.1073/pnas.1700627114.
702 25. Strahl, H., Burmann, F., and Hamoen, L.W. (2014). The actin homologue MreB organizes
703 the bacterial cell membrane. Nat Commun *5*, 3442. 10.1038/ncomms4442.
704 26. Scheinpflug, K., Krylova, O., and Strahl, H. (2017). Measurement of Cell Membrane
705 Fluidity by Laurdan GP: Fluorescence Spectroscopy and Microscopy. Methods Mol Biol
706 *1520*, 159-174. 10.1007/978-1-4939-6634-9_10.
707 27. Lopez, D., and Kolter, R. (2010). Functional microdomains in bacterial membranes. Genes
708 Dev *24*, 1893-1902. 10.1101/gad.1945010.
709 28. Bach, J.N., and Bramkamp, M. (2013). Flotillins functionally organize the bacterial
710 membrane. Molecular microbiology *88*, 1205-1217. 10.1111/mmi.12252.
711 29. Kuru, E., Hughes, H.V., Brown, P.J., Hall, E., Tekkam, S., Cava, F., de Pedro, M.A., Brun,
712 Y.V., and VanNieuwenhze, M.S. (2012). In Situ probing of newly synthesized peptidoglycan
713 in live bacteria with fluorescent D-amino acids. Angew Chem Int Ed Engl *51*, 12519-12523.
714 10.1002/anie.201206749.
715 30. Peschel, A., Otto, M., Jack, R.W., Kalbacher, H., Jung, G., and Gotz, F. (1999). Inactivation
716 of the dlt operon in Staphylococcus aureus confers sensitivity to defensins, protegrins, and
717 other antimicrobial peptides. The Journal of biological chemistry *274*, 8405-8410.
718 10.1074/jbc.274.13.8405.
719 31. Bertsche, U., Yang, S.J., Kuehner, D., Wanner, S., Mishra, N.N., Roth, T., Nega, M.,
720 Schneider, A., Mayer, C., Grau, T., et al. (2013). Increased cell wall teichoic acid production
721 and D-alanylation are common phenotypes among daptomycin-resistant methicillin-

722 resistant Staphylococcus aureus (MRSA) clinical isolates. PloS one *8*, e67398.
723 10.1371/journal.pone.0067398.
724 32. Mishra, N.N., Bayer, A.S., Weidenmaier, C., Grau, T., Wanner, S., Stefani, S., Cafiso, V.,
725 Bertuccio, T., Yeaman, M.R., Nast, C.C., and Yang, S.J. (2014). Phenotypic and genotypic
726 characterization of daptomycin-resistant methicillin-resistant Staphylococcus aureus
727 strains: relative roles of mprF and dlt operons. PloS one *9*, e107426.
728 10.1371/journal.pone.0107426.
729 33. Monteiro, J.M., Fernandes, P.B., Vaz, F., Pereira, A.R., Tavares, A.C., Ferreira, M.T.,
730 Pereira, P.M., Veiga, H., Kuru, E., VanNieuwenhze, M.S., et al. (2015). Cell shape
731 dynamics during the staphylococcal cell cycle. Nat Commun *6*, 8055.
732 10.1038/ncomms9055.
733 34. Wang, Y., Hu, M., Liu, Q., Qin, J., Dai, Y., He, L., Li, T., Zheng, B., Zhou, F., Yu, K., et al.
734 (2016). Role of the ESAT-6 secretion system in virulence of the emerging community-
735 associated Staphylococcus aureus lineage ST398. Sci Rep *6*, 25163. 10.1038/srep25163.
736 35. Garces, A., Atmakuri, K., Chase, M.R., Woodworth, J.S., Krastins, B., Rothchild, A.C.,
737 Ramsdell, T.L., Lopez, M.F., Behar, S.M., Sarracino, D.A., and Fortune, S.M. (2010). EspA
738 acts as a critical mediator of ESX1-dependent virulence in Mycobacterium tuberculosis by
739 affecting bacterial cell wall integrity. PLoS pathogens *6*, e1000957.
740 10.1371/journal.ppat.1000957.
741 36. Ates, L.S., van der Woude, A.D., Bestebroer, J., van Stempvoort, G., Musters, R.J., Garcia-
742 Vallejo, J.J., Picavet, D.I., Weerd, R., Maletta, M., Kuijl, C.P., et al. (2016). The ESX-5
743 System of Pathogenic Mycobacteria Is Involved In Capsule Integrity and Virulence through
744 Its Substrate PPE10. PLoS pathogens *12*, e1005696. 10.1371/journal.ppat.1005696.
745 37. Nath, Y., Ray, S.K., and Buragohain, A.K. (2018). Essential role of the ESX-3 associated
746 eccD3 locus in maintaining the cell wall integrity of Mycobacterium smegmatis.

747 International journal of medical microbiology : IJMM *308*, 784-795.
748 10.1016/j.ijmm.2018.06.010.
749 38. Bosserman, R.E., and Champion, P.A. (2017). Esx Systems and the Mycobacterial Cell
750 Envelope: What's the Connection? Journal of bacteriology *199*. 10.1128/JB.00131-17.
751 39. Bottai, D., Di Luca, M., Majlessi, L., Frigui, W., Simeone, R., Sayes, F., Bitter, W., Brennan,
752 M.J., Leclerc, C., Batoni, G., et al. (2012). Disruption of the ESX-5 system of
753 Mycobacterium tuberculosis causes loss of PPE protein secretion, reduction of cell wall
754 integrity and strong attenuation. Molecular microbiology *83*, 1195-1209. 10.1111/j.1365-
755 2958.2012.08001.x.
756 40. Bramkamp, M., and Lopez, D. (2015). Exploring the existence of lipid rafts in bacteria.
757 Microbiol Mol Biol Rev *79*, 81-100. 10.1128/MMBR.00036-14.
758 41. Grein, F., Muller, A., Scherer, K.M., Liu, X., Ludwig, K.C., Klockner, A., Strach, M., Sahl,
759 H.G., Kubitscheck, U., and Schneider, T. (2020). Ca(2+)-Daptomycin targets cell wall
760 biosynthesis by forming a tripartite complex with undecaprenyl-coupled intermediates and
761 membrane lipids. Nat Commun *11*, 1455. 10.1038/s41467-020-15257-1.
762 42. Rostovtseva, T.K., Aguilella, V.M., Vodyanoy, I., Bezrukov, S.M., and Parsegian, V.A.
763 (1998). Membrane surface-charge titration probed by gramicidin A channel conductance.
764 Biophys J *75*, 1783-1792. 10.1016/S0006-3495(98)77620-9.
765 43. Bobrovskyy, M., Chen, X., and Missiakas, D. (2023). The Type 7b Secretion System of S.
766 aureus and Its Role in Colonization and Systemic Infection. Infection and immunity *91*,
767 e0001523. 10.1128/iai.00015-23.
768 44. Shariati, A., Dadashi, M., Moghadam, M.T., van Belkum, A., Yaslianifard, S., and Darban-
769 Sarokhalil, D. (2020). Global prevalence and distribution of vancomycin resistant,
770 vancomycin intermediate and heterogeneously vancomycin intermediate Staphylococcus
771 aureus clinical isolates: a systematic review and meta-analysis. Sci Rep *10*, 12689.
772 10.1038/s41598-020-69058-z.

773 45. Goodman, J.K., Zampronio, C.G., Jones, A.M.E., and Hernandez-Fernaud, J.R. (2018).
774 Updates of the In-Gel Digestion Method for Protein Analysis by Mass Spectrometry.
775 Proteomics *18*, e1800236. 10.1002/pmic.201800236.
776 46. Ritchie, M.E., Phipson, B., Wu, D., Hu, Y., Law, C.W., Shi, W., and Smyth, G.K. (2015).
777 limma powers differential expression analyses for RNA-sequencing and microarray
778 studies. Nucleic Acids Res *43*, e47. 10.1093/nar/gkv007.
779
780
781
782
783
784
785
786
787
788
789
790
791
792
793
794
795
796
797
798

799 **Figure Legends**

800 **Figure 1. T7SS mutants are more sensitive to membrane acting drugs.**

801 **(A)** Growth curves of WT USA300 JE2, Δ*esxC* and Δ*essC* in TSB in the presence of 5 µg/ml
802 daptomycin and 1 mM $CaCl_2$. Mean ± standard error of the mean (SEM) is shown, N = 3. **(B)** The
803 area under the curve (AUC) of biological replicates in (A) was calculated, mean ± standard
804 deviation (SD) plotted, * P ≤ 0.05, ** P ≤ 0.01 **(C)** CFU/ml was calculated after 8 h daptomycin
805 treatment. N = 3, mean ± SD, *** P≤0.001 using a one-way ANOVA. **(D)** Growth curves of WT
806 pOS1, Δ*esxC* pOS1 and complemented strain Δ*esxC* pOS1-*esxC* in TSB supplemented with 5
807 µg/ml daptomycin and 1 mM $CaCl_2$. Mean ± SEM shown, N = 3.; AUC was calculated and the
808 mean ± SD plotted in **(E)** * P ≤ 0.05. **(F)** CFU/ml from a killing assay in the presence of 10 µg/ml
809 daptomycin and 1mM $CaCl_2$ at timepoints indicated. **(G)** CFU/ml from killing assay using WT
810 USA300 JE2, Δ*esxC* and Δ*esxC* complemented strains of in the presence of 10 µg/ml daptomycin
811 and 1mM $CaCl_2$ at timepoints indicated, mean ± SD, N = 3, * P ≤ 0.05, ** P ≤ 0.01, *** P ≤ 0.001
812 using a two-way ANOVA with Tukey multiple comparison test. (H) Growth curves of USA300 JE2
813 WT, *ΔessC* and Δ*esxC* in the presence of 2 µg/ml gramicidin, Mean ± SEM, N = 3 (I) Growth
814 curves of USA300 JE2 WT, *ΔessC* and Δ*esxC* in the presence of 1 µg/ml bithionol. Mean ± SEM,
815 N = 3.

816

817 **Figure 2. T7SS affects membrane fluidity and protein localisation.**

818 A) The membrane fluidity of WT USA300 JE2 and Δ*esxC* as measured with a pyrene decanoic
819 acid staining-based assay. Mean ± SEM are shown, N = 6, * indicates P < 0.05 using a two-tailed
820 t-test. B) Widefield micrographs of *S. aureus* WT and Δ*esxC* after growth in TSB to OD_{600} of 1.0
821 in the presence of the lipophilic dye DiIC12. Images are representative of 4 independent
822 experiments. The DiIC12 fluorescence of 80 bacterial clusters from different fields per strain was
823 quantitated with ImageJ. Means ± SD are shown, N = 4; **** P < 0.0001, using a Kruskal-Wallis
824 rank test. C) One point measurement of fluidity in logarithmic phase *S. aureus* WT and *ΔesxC*,

825 grown in TSB at 37ºC. Laurdan generalised polarisation (GP) was calculated using the equation
826 $(I_{460} – I_{500})/ (I_{460} – I_{500})$ where I refers to the fluorescent intensity at the emission wavelength. *** P
827 = 0.0003 using an unpaired t-test with Welch's correction, N=3, mean ± SD. D) Representative
828 widefield microscopy images of FloA-eYFP expressing WT and T7SS mutant strains.
829 Deconvolved images were acquired using a Deltavision microscope. N=3. Quantification of the
830 number of foci per cell (n = 100 per mutant).
831
832 **Figure 3. T7SS mutants have distinct surface morphologies.**
833 A) Representative SEM images of *S. aureus* WT USA300 JE2, *ΔessC*, *ΔesxC*, and *ΔesxD*
834 bacteria grown to early logarithmic phase. B) Representative SEM images of *S. aureus* USA300
835 JE2 WT pOS1, *ΔesxC* pOS1, *ΔesxC* pOS1 *esxC* grown to early logarithmic phase.
836
837 **Figure 4. T7SS impacts cell wall synthesis.**
838 (A) Representative widefield micrographs of *S. aureus* cultures either grown to logarithmic phase
839 in the presence of 25 μM HADA or after 10-minute treatment with HADA once OD_{600} of 1 was
840 reached. (B) Quantification of fluorescence in cells grown to logarithmic phase with HADA. (C)
841 Quantification of fluorescence in cells treated with HADA for 10 min Quantification performed on
842 five images each from 3 independent experiments. ** = P< 0.01, and **** =P < 0.0001 by One-
843 way ANOVA.
844
845 **Figure 5. T7SS mutant membranes bind more to daptomycin.**
846 Quantitative binding assay of cytochrome C to WT USA300 JE2, Δ*esxC* and Δ*essC* and WT
847 USA300 LAC, *ΔesxA*, Δ*esxB* mutants (A, C). The CFU of the starting inoculum was calculated for
848 each mutant (B, D). Mean ± SD shown (N = 3), ***P < 0.001 using a one-way ANOVA. E)
849 Fluorescence measurements of daptomycin-BODIPY binding to *S. aureus.* The excitation
850 wavelength was 488nm and emission wavelength was 530nm. N=3, mean ± SD. P = 0.0067,

851 using an unpaired t-test. F) Representative micrograph of daptomycin-BODIPY binding to *S.*
852 *aureus.*
853
854 **Figure 6. T7SS mutant membranes are more permeable in the presence of daptomycin**
855 A) Representative fluorescent micrographs of *S. aureus* T7SS mutants treated with daptomycin.
856 Cell membranes were stained by FM1-43 and imaged using FITC filter channel, PI was imaged
857 using Texas red filter channel and the DAPI was imaged using DAPI filter set. B) Images were
858 quantified using FIJI. Data presented is from 3 independent experiments. 10 images from each
859 experiment were quantified and normalised to the number of cells in the field of view. Statistical
860 analysis performed using an ANOVA * $P \leq 0.05$, ** $P \leq 0.01$.
861
862 **Figure 7. Presence of T7SS affects intracellular bacterial killing by daptomycin.**
863 A) CFU counts at various timepoints during the infection assay. 0 h represents the initial inoculum,
864 1 h represents the CFU counts that have infected the cell and 4 h and 24 h represent the survival
865 of *S. aureus* in the presence of daptomycin, N = 3, **$P<0.05$, two-way ANOVA. (B) Confocal image
866 quantification from five images each from 3 independent experiments. Mean ± SD of intensity, is
867 shown, ***$P<0.01$ using a one-way ANOVA. (C) Representative confocal micrographs of cells after
868 1 h infection or 24 h post-infection. DAPI (blue), F-actin (red), and *S. aureus* (green, white arrows).
869
870 **Figure 8. EsxC mutants are more sensitive to daptomycin *in vivo.***
871 Skin-abscess model mice (n=8, 2 lesions/animal) were infected with WT USA300 and Δ*esxC*
872 mutant followed by treatment with 10 mg/kg daptomycin. (A) CFU/g skin tissue was calculated 24
873 h post infection. Graphs show mean ± SD, P = 0.0007 using one-way ANOVA (B) CFU//g was
874 calculated 72 h post infection (n=5, 2 lesions/animal), mean ± SD shown, P = 0.0020 using a one-
875 way ANOVA. (C) TNF-α levels: Two-way ANOVA revealed a significant effect on treatment groups

876 (P <0.01). Results of multiple comparisons shown on graph. (D) IL-1β levels, but significant effect
877 seen between treatment groups (P<0.01) using two-way ANOVA. Graphs show mean ± SD, n=5.
878
879
880
881
882
883
884
885
886
887
888
889
890
891
892
893

894 **Table 1.** Proteins significantly changed in Δ*esxC* and Δ*essC* mutant membrane preparations

895 relative to WT USA300 JE2. Proteins common to both mutants are in bold.

	Uniprot ID	$\log_2$ fold change	Adjusted *P* value	Description
USA300 JE2 Δ*esxC* vs USA300 JE2 WT	A0A0H2XJR2	-5.46	6.21E-08	Pyridine nucleotide-disulfide oxidoreductase
	A0A0H2XJ15	**-5.34**	**3.80E-09**	**TPR domain protein**
	A0A0H2XIV9	-5.33	1.49E-07	T7SS protein, EssD
	A0A0H2XJ90	-4.82	6.92E-09	D-isomer specific 2-hydroxyacid dehydrogenase family protein
	A0A0H2XF36	**3.62**	**2.14E-08**	**Uncharacterised protein**
	A0A0H2XJV3	**3.67**	**2.26E-08**	**ABC transporter, ATP-binding protein**
	A0A0H2XGS2	3.70	1.71E-08	Putative sensor histidine kinase
	A0A0H2XG87	**4.01**	**1.59E-08**	**Bifunctional ligase/repressor BirA**
	A0A0H2XH85	4.14	1.04E-08	Cobalamin synthesis protein/P47K family protein
	A0A0H2XER9	4.38	9.36E-09	LysR family regulatory protein
	A0A0H2XEB7	**5.25**	**2.39E-07**	**Integral membrane protein**
	A0A0H2XJ96	**5.27**	**1.04E-08**	**NADH-dependent flavin oxidoreductase**
	A0A0H2XHU5	5.97	2.55E-09	Putative membrane protein
USA300 JE2 Δ*essC* vs USA300 JE2 WT	A0A0H2XEV3	-8.65	3.31E-08	T7SS protein, EssC
	A0A0H2XJ15	-5.34	5.71E-09	TPR domain protein
	A0A0H2XH73	-4.56	2.19E-08	NAD-dependent epimerase-domain-containing protein
	A0A0H2XFR1	3.33	2.52E-08	Energy-coupling factor transporter transmembrane protein EcfT
	A0A0H2XJF9	3.47	2.19E-08	Putative deoxyribodipyrimidine photolyase
	A0A0H2XF36	3.57	2.19E-08	Uncharacterised protein
	A0A0H2XJV3	3.59	2.42E-08	ABC transporter, ATP-binding protein
	A0A0H2XG87	3.93	1.82E-08	Bifunctional ligase/repressor BirA
	A0A0H2XGW9	4.26	9.38E-09	Deoxynucleoside kinase family protein
	A0A0H2XIK4	4.46	8.12E-09	ornithine aminotransferase
	A0A0H2XHF0	4.56	8.12E-09	Carboxylic ester hydrolase
	A0A0H2XHR8	4.80	8.12E-09	DJ-1/PfpI domain-containing protein

	A0A0H2XEB7	4.82	4.09E-07	Integral membrane protein
	A0A0H2XJ96	4.83	1.82E-08	NADH-dependent flavin oxidoreductase
	A0A0H2XEH0	8.22	5.27E-10	Alpha, alpha-phosphotrehalase

896

897 **Table 2. Strains and Plasmids used in this study**

Strain or Plasmid	Description	Source or Reference
Staphylococcus aureus		
USA300 LAC JE2	Plasmid-cured USA300 LAC	BEI Resources (NARSA)
USA300 JE2 *ΔessC*	USA300 LAC JE2 defective for EssC	(Kengmo Tchoupa *et al.,* 2020)
USA300 JE2 *ΔesxC*	USA300 LAC JE2 defective for EsxC	(Kengmo Tchoupa *et al.,* 2020)
USA300 LAC	Community acquired MRSA	(Bae and Schneewind, 2006)
USA300 LAC *ΔesxA*	USA300 LAC defective for EsxA	(Korea *et al.,* 2014)
USA300 LAC Δ*esxB*	USA300 LAC defective for EsxB	(Korea *et al.,* 2014)
Newman	Methicillin-sensitive *S. aureus*	(Bae and Schneewind, 2006)
Newman *ΔesxA*	Newman defective for EsxA	(Korea *et al.,* 2014)
Newman Δ*esxB*	Newman defective for EsxB	(Korea *et al.,* 2014)
RN6390	NCTC8325 derivative, *ΔrbsU, ΔtcaR,* cured of φ11, φ12, and φ13	Tracy Palmer (Kneuper *et al.,* 2014)
RN6390 *ΔessC*	RN6390 defective for EssC	Tracy Palmer (Kneuper *et al.,* 2014)
RN6390 *ΔesxC*	RN6390 defective for EsxC	Tracy Palmer (Kneuper *et al.,* 2014)
Plasmids		
pOS1	Empty vector for complementation	(Kengmo Tchoupa *et al.,* 2020)
pOS1-*esxC*	*esxC* complementation vector	(Kengmo Tchoupa *et al.,* 2020)

898

899

900

901

902

903 **Supplementary Figure legends and tables**

904 **Figure S1.** Growth curves of (A) USA300 JE2 WT, *ΔessC,* Δ*esxC* and *ΔesxD* (B) USA300JE2 WT
905 pOS1, Δ*esxC* pOS1 and complemented strain Δ*esxC* pOS1-*esxC* C) RN6390 WT, *ΔessC* and
906 Δ*esxC* (D) Newman WT and Δ*esxA* and *ΔesxB* mutants (E) USA300 LAC WT and Δ*esxA* and
907 Δ*esxB* grown in TSB at 37ºC. OD_{600} measured every 15 min. Mean ± SEM plotted on graph, N=3.

908

909 **Figure S2**. Growth curves of (A) USA300 JE2 WT, and Δ*esxD*, (C) RN6390 WT, *ΔessC* and
910 Δ*esxC*, (E) USA300 Δ*esxA* and Δ*esxB* and (G) Newman Δ*esxA* and *ΔesxB* in TSB in the presence
911 of 5 µg/ml daptomycin and 1 mM $CaCl_2$. Mean ± SEM are shown, N = 3. The AUC was calculated
912 and the mean ± SD was plotted for the growth curve shown on the left (B, D, F, H). * $P \leq 0.05$, **
913 $P \leq 0.01$.

914

915 **Figure S3**. Growth curves of USA300 JE2 WT, *ΔessC* and Δ*esxC* in the presence of (A) 4 µg/ml
916 ciprofloxacin (B) 0.5 µg/ml mitomycin C. (C) 1 µg/ml oxacillin. (D) 8 µg/ml vancomycin. For all
917 growth curves mean and SEM are shown, N = 3.

918

919 **Figure S4.** Scanning electron micrographs of *S. aureus* RN6390, USA300, and Newman T7SS
920 mutants.

921

922 **Figure S5** Transmission electron micrographs of *S. aureus* USA300 JE2 WT, Δ*essC* and Δ*esxC*
923 grown to early logarithmic phase.

924

925 **Figure S6** (A) Growth curves of WT, ΔessC and Δ*esxC* in DMEM + FBS. **(B)** Growth curves of
926 WT, Δ*essC* and ΔesxC in DMEM + FBS in the presence of 1µg/ml daptomycin and 1 mM $CaCl_2$.
927 Graphs show mean and SEM of three independent experiments.

928

929 **Figure S7** The area of lesions was measured and calculated daily from mice infected with *S.*
930 *aureus* WT or T7SS mutants. Area of lesions was measured and calculated daily. Graphs show
931 mean ± SD. Two-way ANOVA between groups revealed no significant differences between
932 treatments.

933 **Table S**1 Secreted proteins significantly changed in Δ*esxC* and Δ*essC* mutants relative to WT
934 USA300 JE2.

935

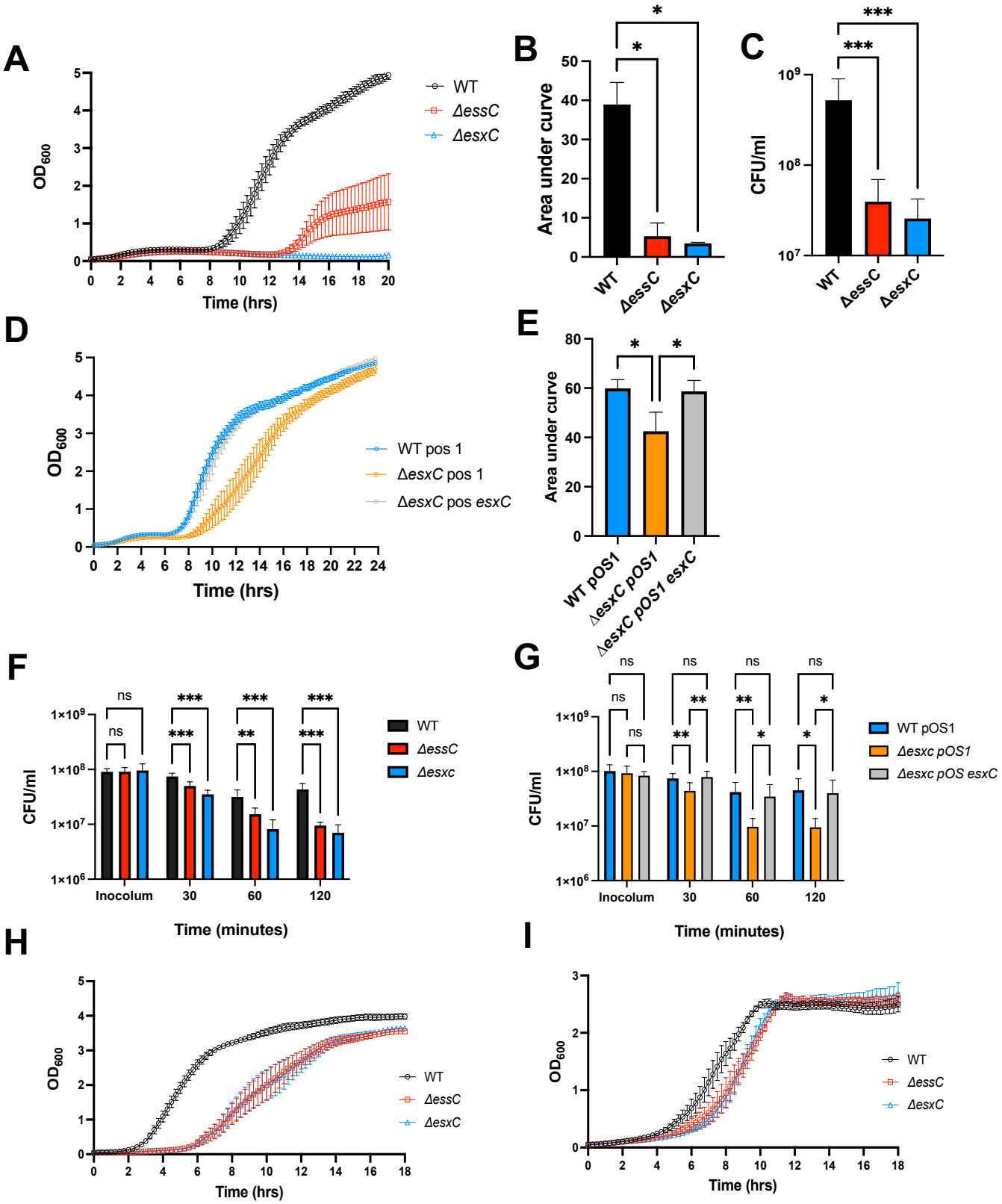

Figure 1. T7SS mutants are more sensitive to membrane acting drugs.
(A) Growth curves of WT USA300 JE2, Δ*esxC* and Δ*essC* in TSB in the presence of 5 µg/ml daptomycin and 1 mM $CaCl_2$. Mean ± standard error of the mean (SEM) is shown, N = 3. **(B)** The area under the curve (AUC) of biological replicates in (A) was calculated, mean ± standard deviation (SD) plotted, * P ≤ 0.05, ** P ≤ 0.01 **(C)** CFU/ml was calculated after 8 h daptomycin treatment. N = 3, mean ± SD, *** P≤0.001 using a one-way ANOVA. **(D)** Growth curves of WT pOS1, Δ*esxC* pOS1 and complemented strain Δ*esxC* pOS1-*esxC* in TSB supplemented with 5 µg/ml daptomycin and 1 mM $CaCl_2$. Mean ± SEM shown, N = 3.; AUC was calculated and the mean ± SD plotted in **(E)** * P ≤ 0.05. **(F)** CFU/ml from a killing assay in the presence of 10 µg/ml daptomycin and 1mM $CaCl_2$ at timepoints indicated. **(G)** CFU/ml from killing assay using WT USA300 JE2, Δ*esxC* and Δ*esxC* complemented strains of in the presence of 10 µg/ml daptomycin and 1mM $CaCl_2$ at timepoints indicated, Mean ± SD,N = 3, * P ≤ 0.05, ** P ≤ 0.01, *** P ≤ 0.001 using a two-way ANOVA with Tukey multiple comparison test. (H) Growth curves of USA300 JE2 WT, Δ*essC* and Δ*esxC* in the presence of 2 µg/ml gramicidin, Mean ± SEM, N = 3 (I) Growth curves of USA300 JE2 WT, Δ*essC* and Δ*esxC* in the presence of 1 µg/ml bithionol. Mean ± SEM, N = 3.

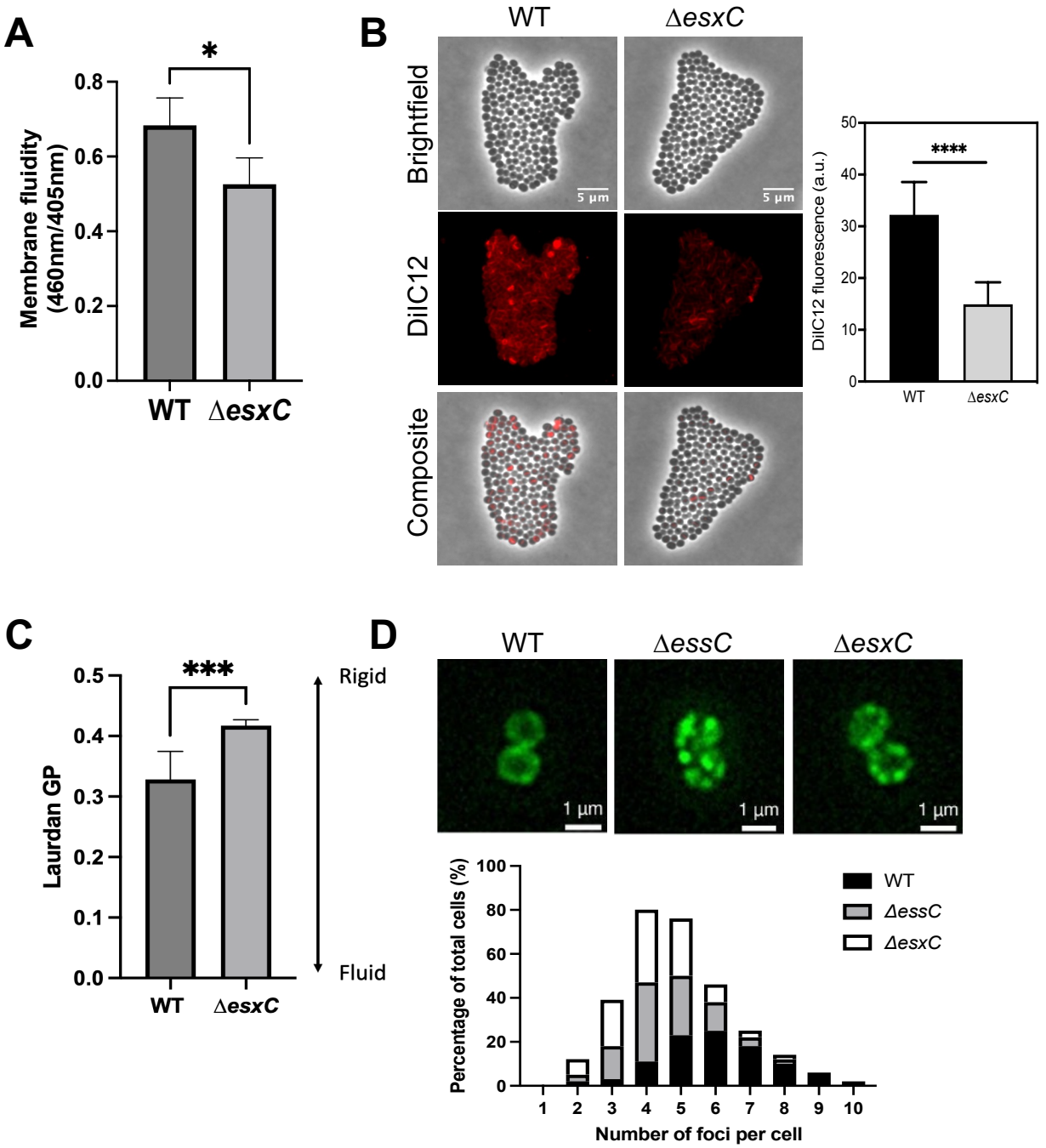

Figure 2. T7SS affects membrane fluidity and protein localisation.

A) The membrane fluidity of WT USA300 JE2 and Δ*esxC* as measured with a pyrene decanoic acid staining-based assay. Mean ± SEM are shown, N = 6, * indicates $P < 0.05$ using a two-tailed t-test. B) Widefield micrographs of *S. aureus* WT and Δ*esxC* after growth in TSB to OD_{600} of 1.0 in the presence of the lipophilic dye DiIC12. Images are representative of 4 independent experiments. The DiIC12 fluorescence of 80 bacterial clusters from different fields per strain was quantitated with ImageJ. Means ± SD are shown, N = 4; **** $P < 0.0001$, using a Kruskal-Wallis rank test. C) One point measurement of fluidity in logarithmic phase *S. aureus* WT and *ΔesxC*, grown in TSB at 37ºC. Laurdan generalised polarisation (GP) was calculated using the equation $(I_{460} – I_{500})/ (I_{460} – I_{500})$ where I refers to the fluorescent intensity at the emission wavelength. *** $P = 0.0003$ using an unpaired t-test with Welch's correction, N=3, mean ± SD. D) Representative widefield microscopy images of FloA-eYFP expressing WT and T7SS mutant strains. Deconvolved images were acquired using a Deltavision microscope. N=3. Quantification of the number of foci per cell (n = 100 per mutant).

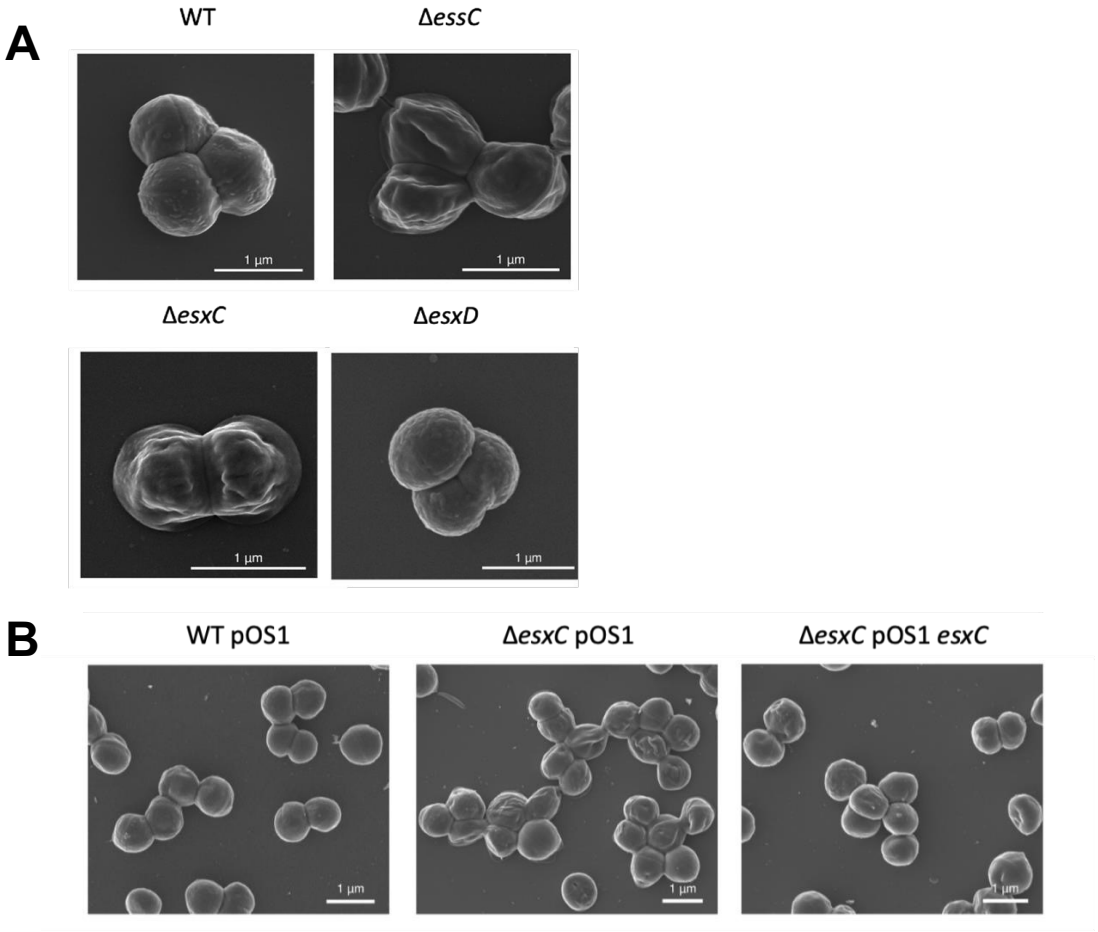

Figure 3. T7SS mutants have distinct surface morphologies.

A) Representative SEM images of *S. aureus* WT USA300 JE2, *ΔessC*, *ΔesxC*, and *ΔesxD* bacteria grown to early logarithmic phase. B) Representative SEM images of *S. aureus* USA300 JE2 WT pOS1, *ΔesxC* pOS1, *ΔesxC* pOS1 *esxC* grown to early logarithmic phase.

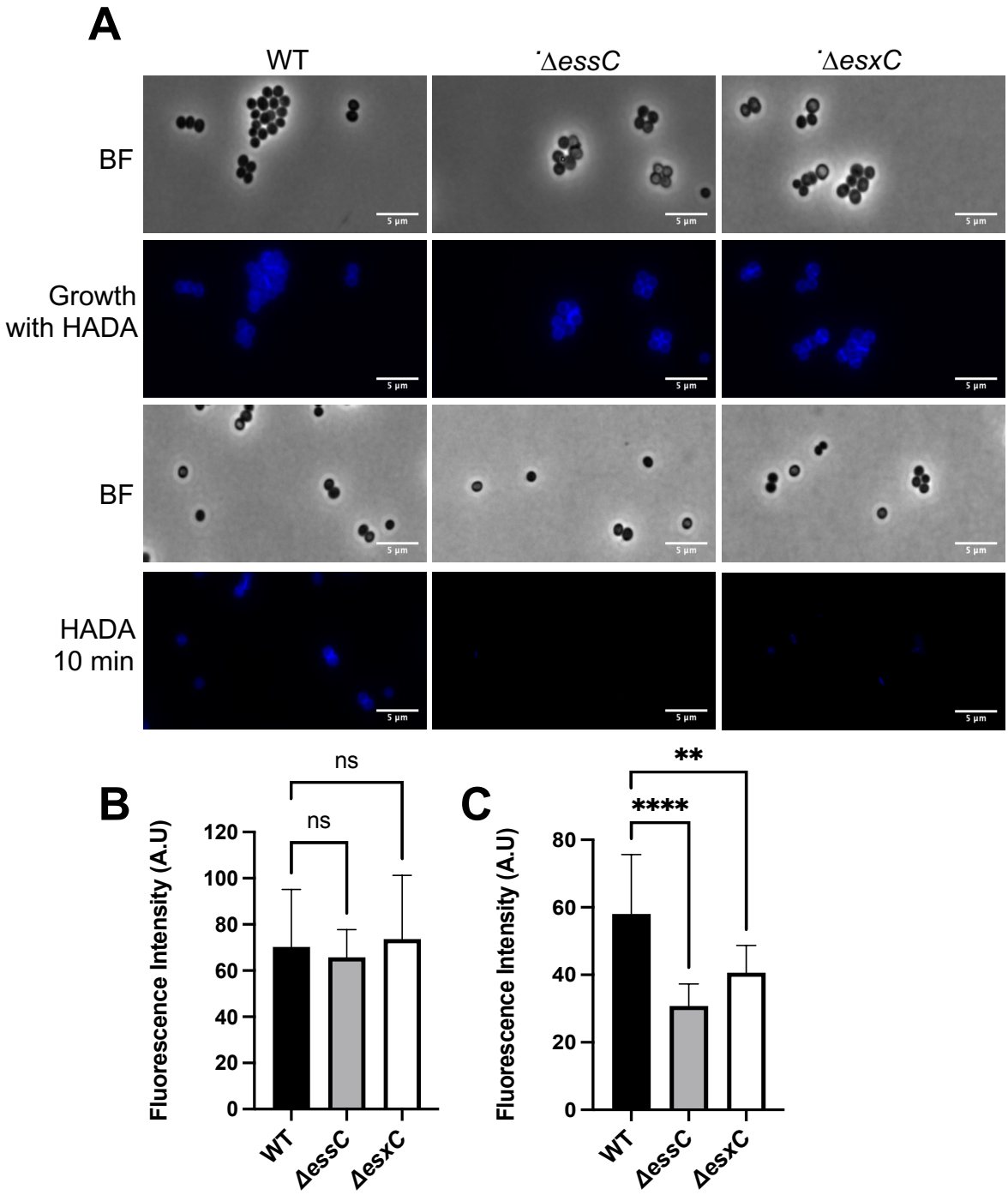

Figure 4. T7SS impacts cell wall synthesis.

(A) Representative widefield micrographs of *S. aureus* cultures either grown to logarithmic phase in the presence of 25 µM HADA or after 10-minute treatment with HADA once OD_{600} of 1 was reached. (B) Quantification of fluorescence in cells grown to logarithmic phase with HADA. (C) Quantification of fluorescence in cells treated with HADA for 10 minutes. Quantification performed on five images each from 3 independent experiments. ** = P< 0.01, and **** =P < 0.0001 by One-way ANOVA

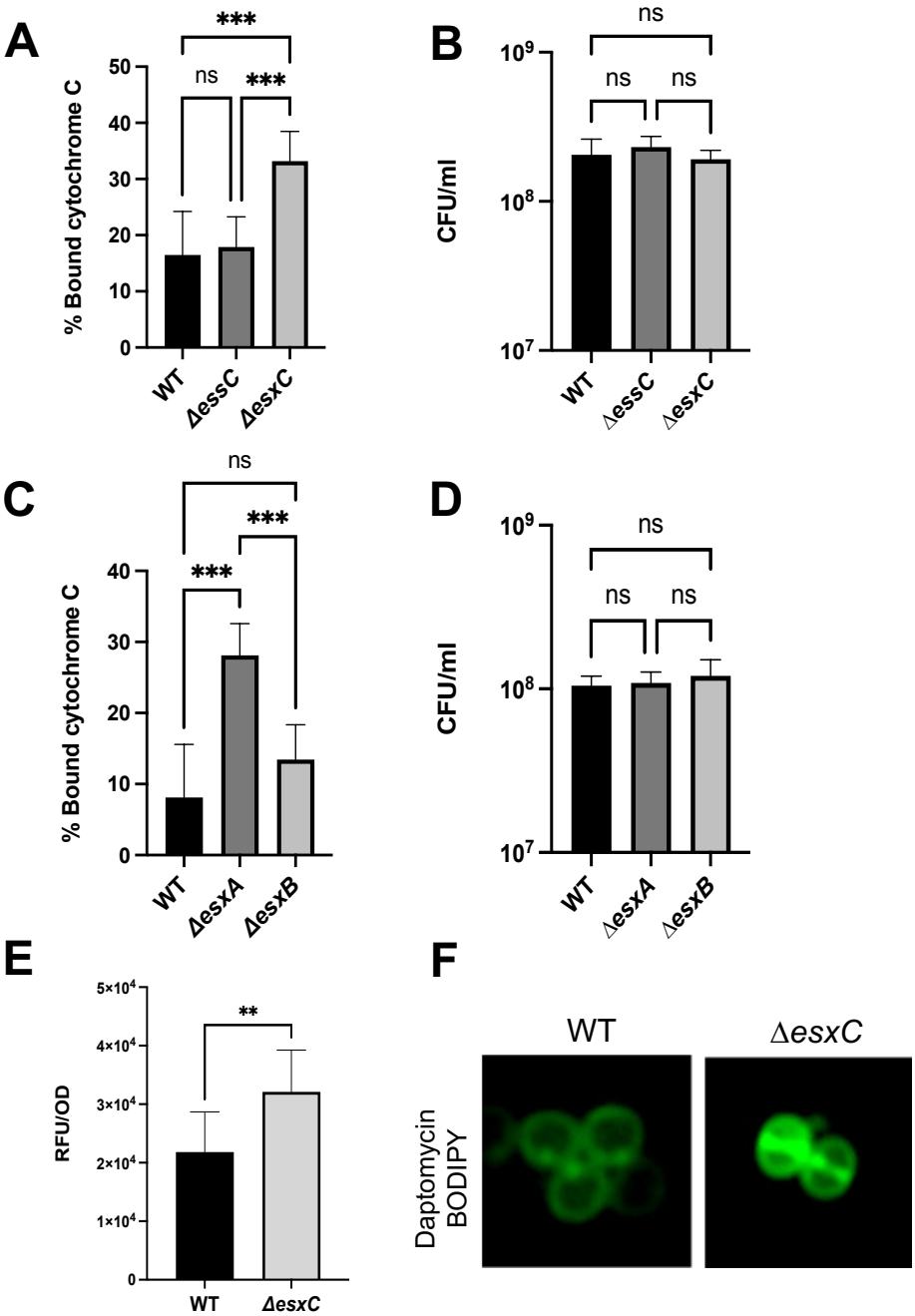

Figure 5. T7SS mutant membranes bind more to daptomycin.
Quantitative binding assay of cytochrome C to WT USA300 JE2, Δ*esxC* and Δ*essC* and WT USA300 LAC, *ΔesxA*, Δ*esxB* mutants (A, C). The CFU of the starting inoculum was calculated for each mutant (B, D). Mean ± SD shown (N = 3), ***P < 0.001 using a one-way ANOVA. E) Fluorescence measurements of daptomycin-BODIPY binding to *S. aureus.* The excitation wavelength was 488nm and emission wavelength was 530nm. N=3, mean ± SD. P = 0.0067, using an unpaired t-test. F) Representative micrograph of daptomycin-BODIPY binding to *S. aureus.*

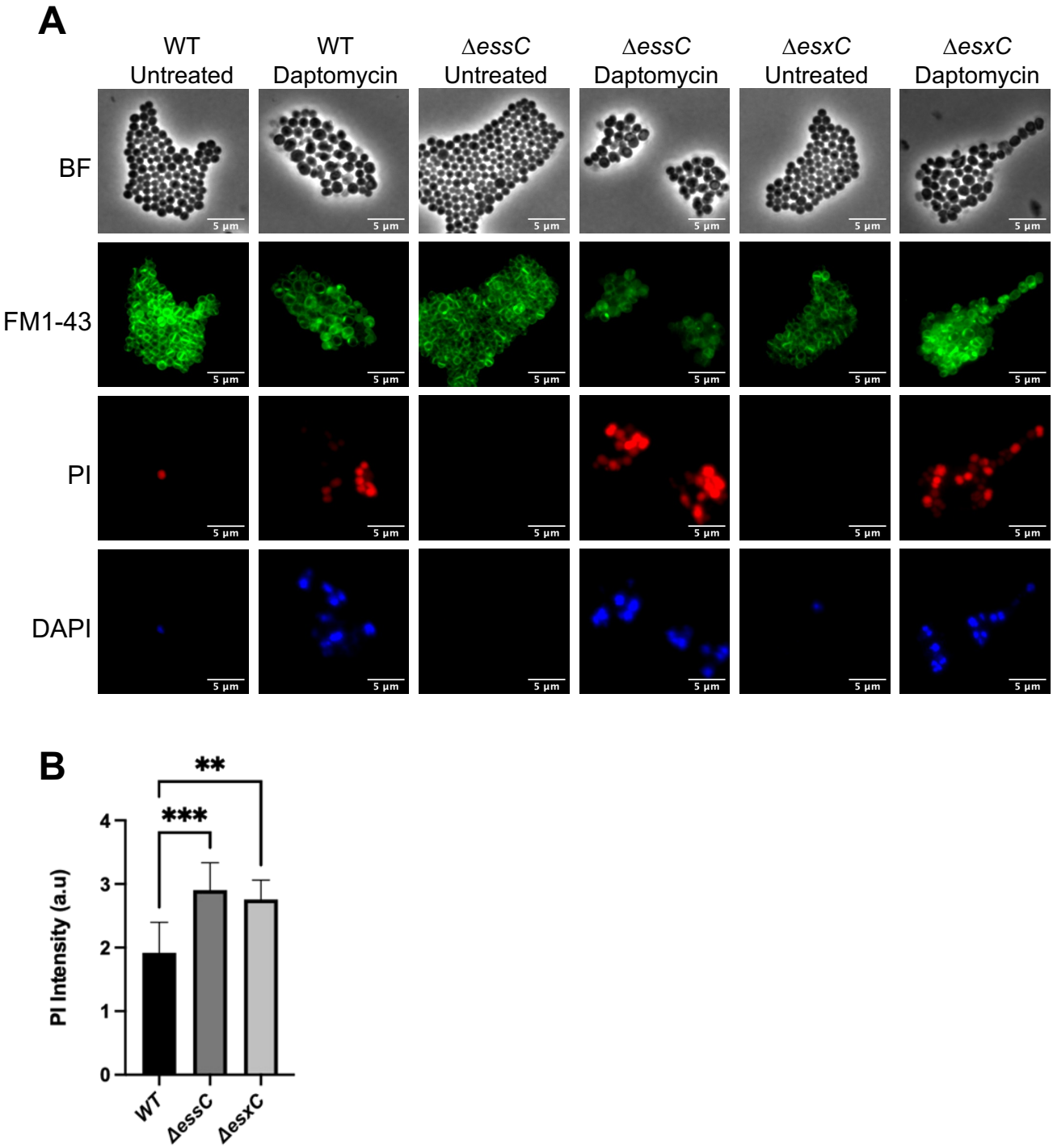

Figure 6. T7SS mutant membranes are more permeable in the presence of daptomycin
A) Representative fluorescent micrographs of *S. aureus* T7SS mutants treated with daptomycin. Cell membranes were stained by FM1-43 and imaged using FITC filter channel, PI was imaged using Texas red filter channel and the DAPI was imaged using DAPI filter set. B) Images were quantified using FIJI. Data presented is from 3 independent experiments. 10 images from each experiment were quantified and normalised to the number of cells in the field of view. Statistical analysis performed using an ANOVA * $P \leq 0.05$, ** $P \leq 0.01$.

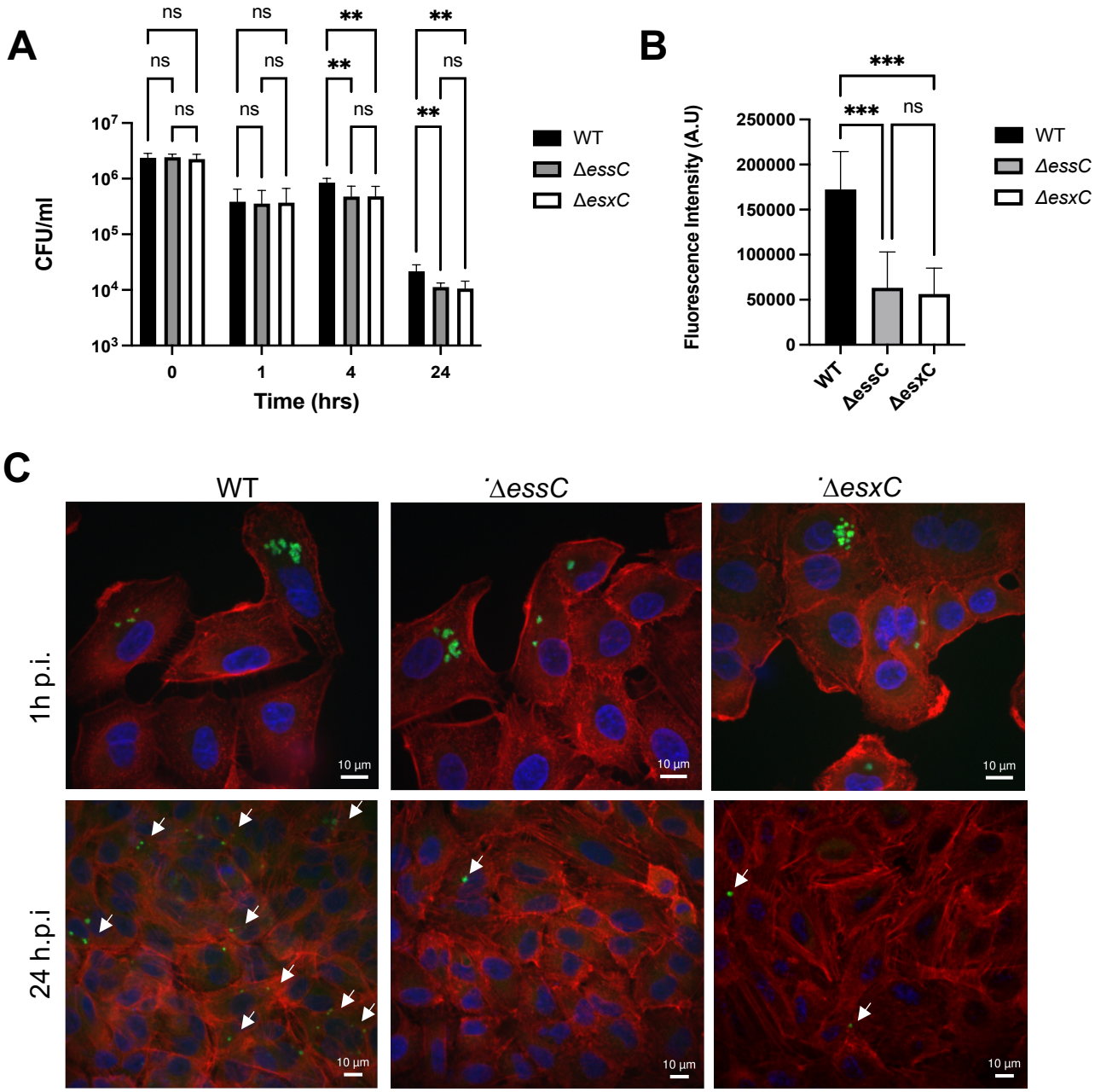

Figure 7. Presence of T7SS affects intracellular bacterial killing by daptomycin. A) CFU counts at various timepoints during the infection assay. 0 h represents the initial inoculum, 1 h represents the CFU counts that have infected the cell and 4 h and 24 h represent the survival of *S. aureus* in the presence of daptomycin, N = 3, **P<0.05, two-way ANOVA. (B) Confocal image quantification from five images each from 3 independent experiments. Mean ± SD of intensity, is shown, ***P<0.01 using a one-way ANOVA. (C) Representative confocal micrographs of cells after 1 h infection or 24 h post-infection. DAPI (blue), F-actin (red), and *S. aureus* (green, white arrows).

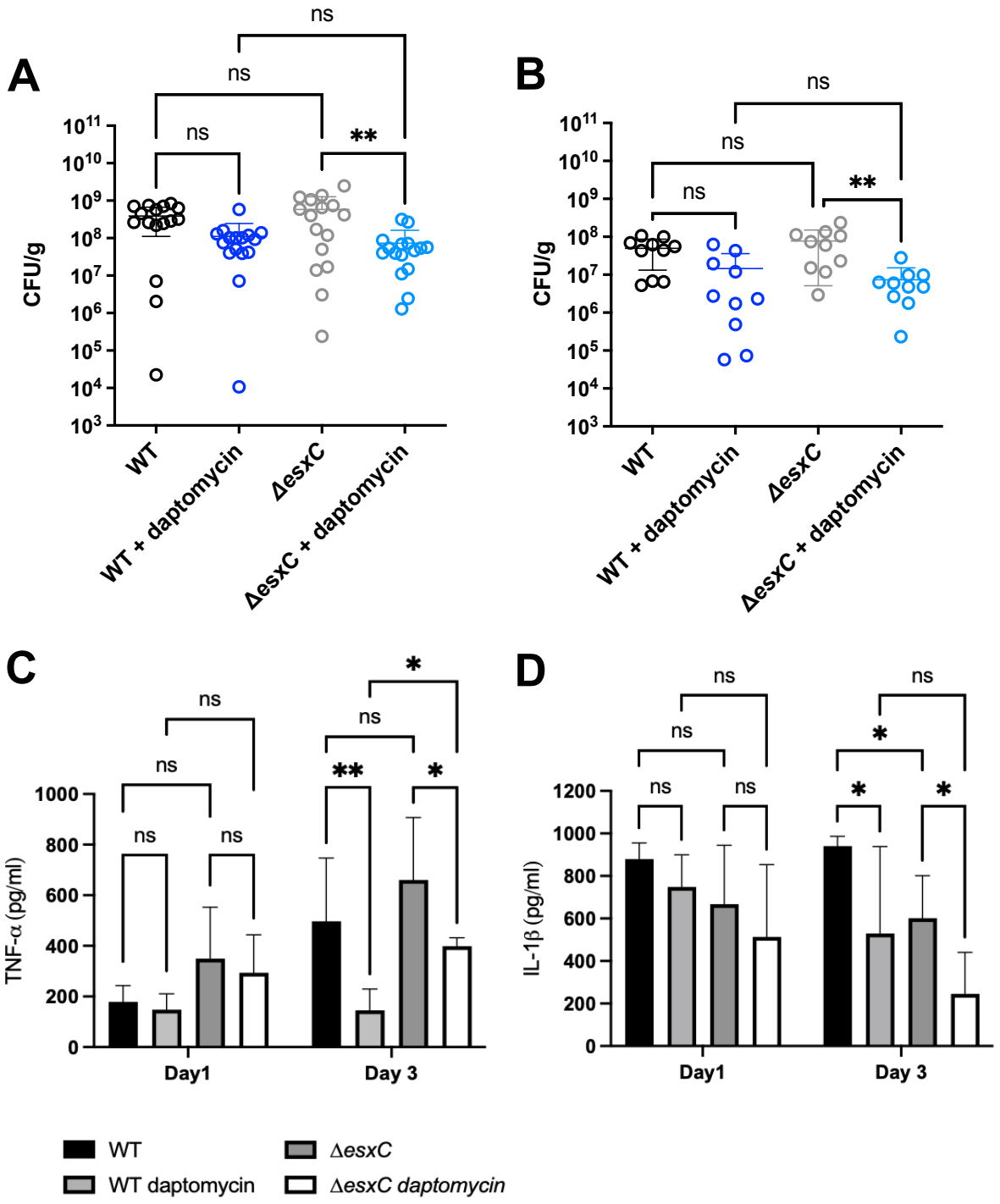

Figure 8. EsxC mutants are more sensitive to daptomycin *in vivo.*
Skin-abscess model mice (n=8, 2 lesions/animal) were infected with WT USA300 and Δ*esxC* mutant followed by treatment with 10 mg/kg daptomycin. (A) CFU/g skin tissue was calculated 24 h post infection. Graphs show mean ± SD, P = 0.0007 using one-way ANOVA (B) CFU//g was calculated 72 h post infection (n=5, 2 lesions/animal), mean ± SD shown, P = 0.0020 using a one-way ANOVA. (C) TNF-α levels: Two-way ANOVA revealed a significant effect treatment groups (P <0.01). Results of multiple comparisons shown on graph. (D) IL-1β levels , but significant effect seen between treatment groups (P<0.01) using two-way ANOVA. Graphs show mean ± SD, n=5.

Fig S1

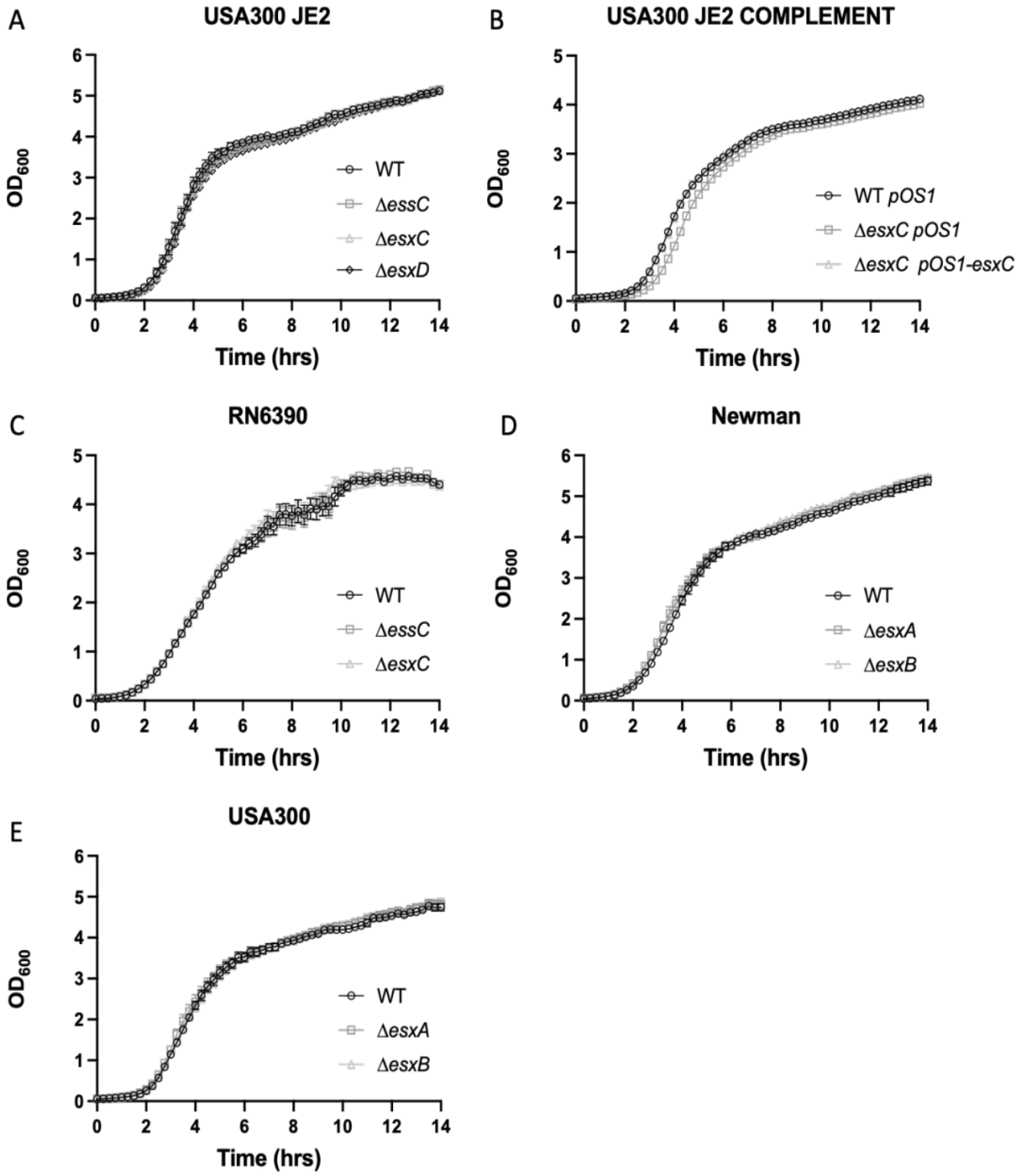

Figure S1. Growth curves of (A) USA300 JE2 WT, *ΔessC,* Δ*esxC* and *ΔesxD* (B) USA300JE2 WT pOS1, Δ*esxC* pOS1 and complemented strain Δ*esxC* pOS1-*esxC* C) RN6390 WT, *ΔessC* and Δ*esxC* (D) Newman WT and Δ*esxA* and *ΔesxB* mutants (E) USA300 LAC WT and Δ*esxA* and Δ*esxB* grown in TSB at 37ºC. OD_{600} measured every 15 minutes. Mean ± SEM plotted on graph, N=3.

Fig S2

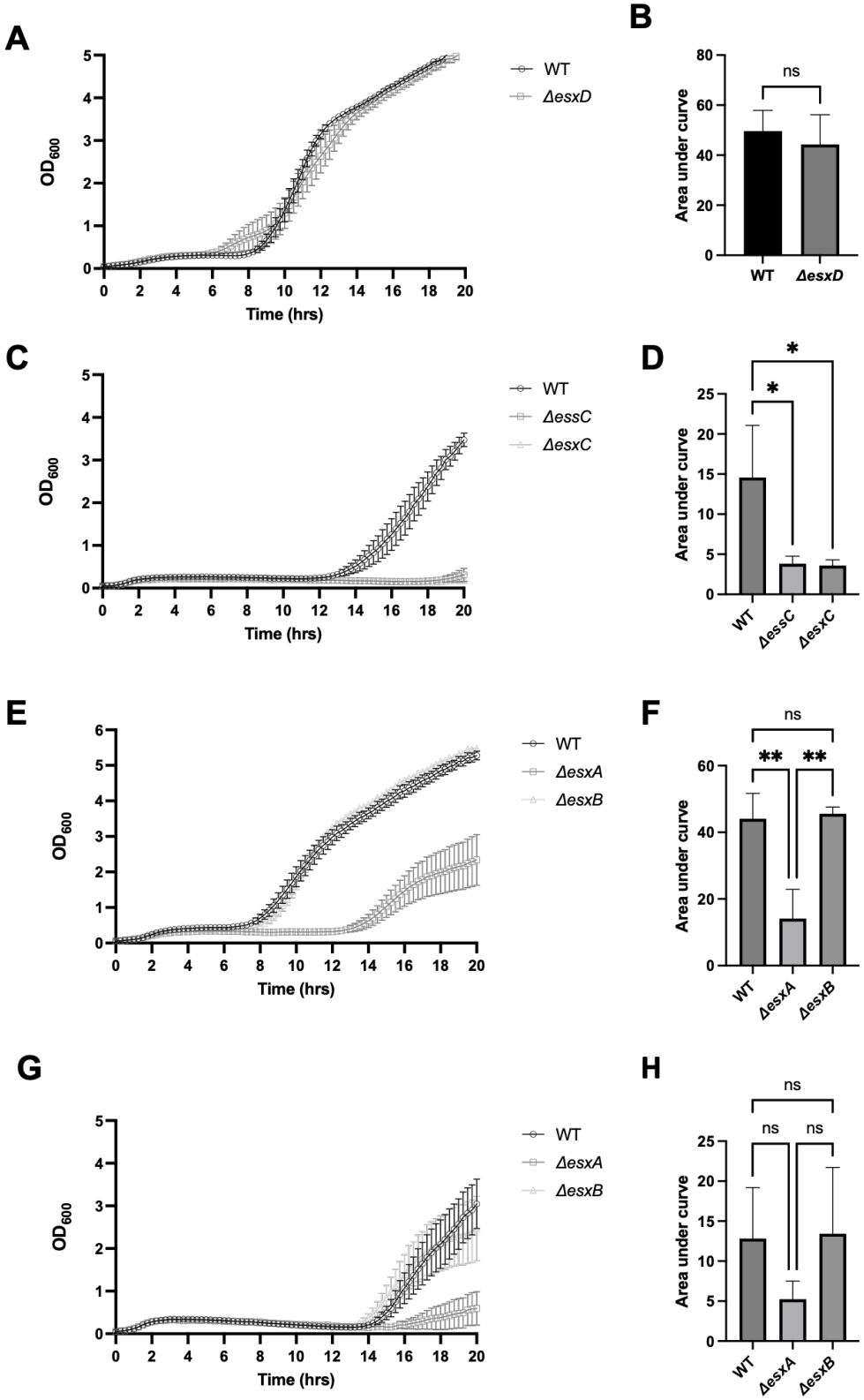

Figure S2. Growth curves of (A) USA300 JE2 WT, and Δ*esxD*, (C) RN6390 WT, *ΔessC* and Δ*esxC*, (E) USA300 Δ*esxA* and Δ*esxB* and (G) Newman Δ*esxA* and *ΔesxB* in TSB in the presence of 5 µg/ml daptomycin and 1 mM $CaCl_2$. Mean ± SEM are shown, N = 3. The AUC was calculated and the mean ± SD was plotted for the growth curve shown on the left (B, D, F, H). * P ≤ 0.05, ** P ≤ 0.01.

Fig S3

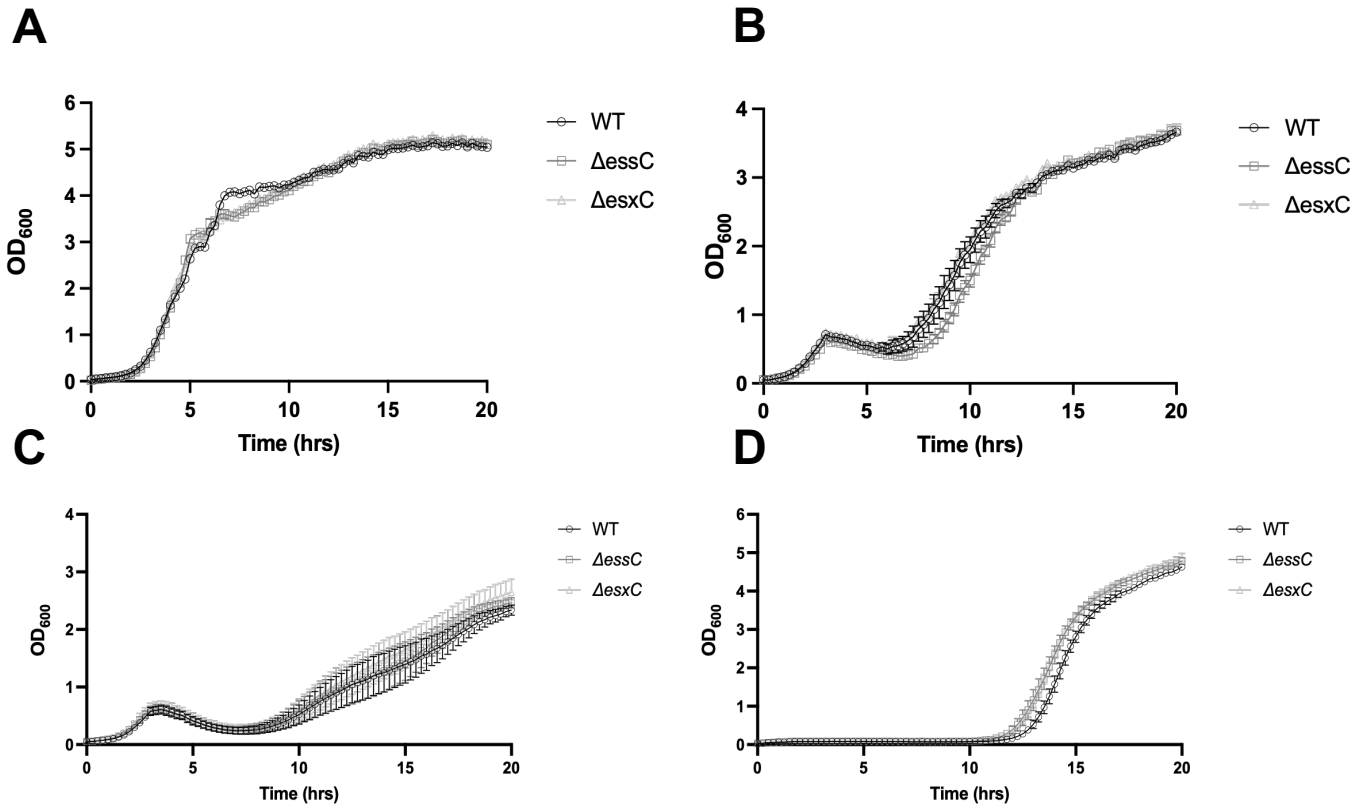

Figure S3. Growth curves of USA300 JE2 WT, *ΔessC* and Δ*esxC* in the presence of (A) 4 µg/ml ciprofloxacin (B) 0.5 µg/ml mitomycin C. (C) 1 µg/ml oxacillin. (D) 8 µg/ml vancomycin. For all growth curves mean and SEM are shown, N = 3.

Fig S4

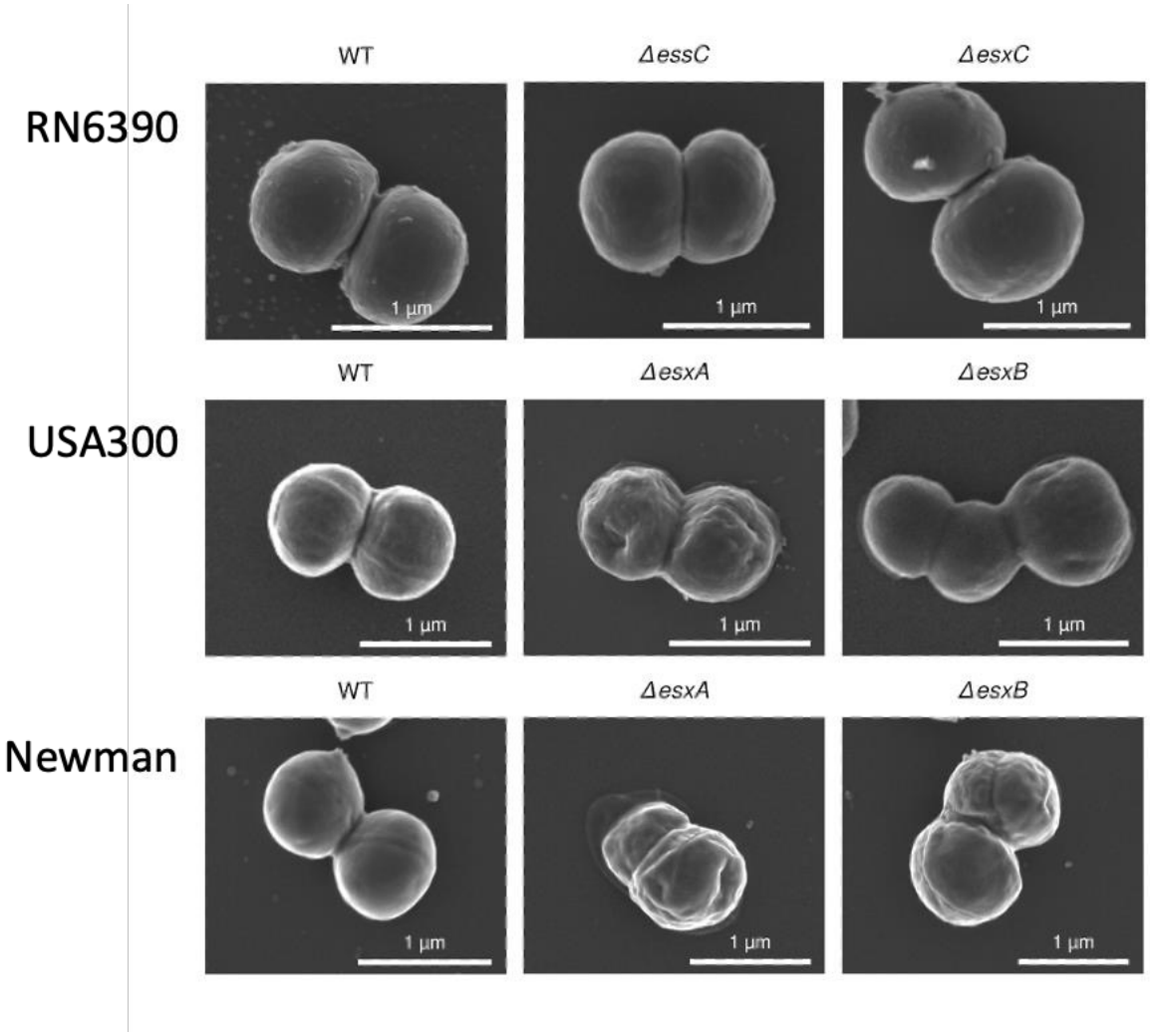

Figure S4. Scanning electron micrographs of *S. aureus* RN6390, USA300, and Newman T7SS mutants.

Fig S5

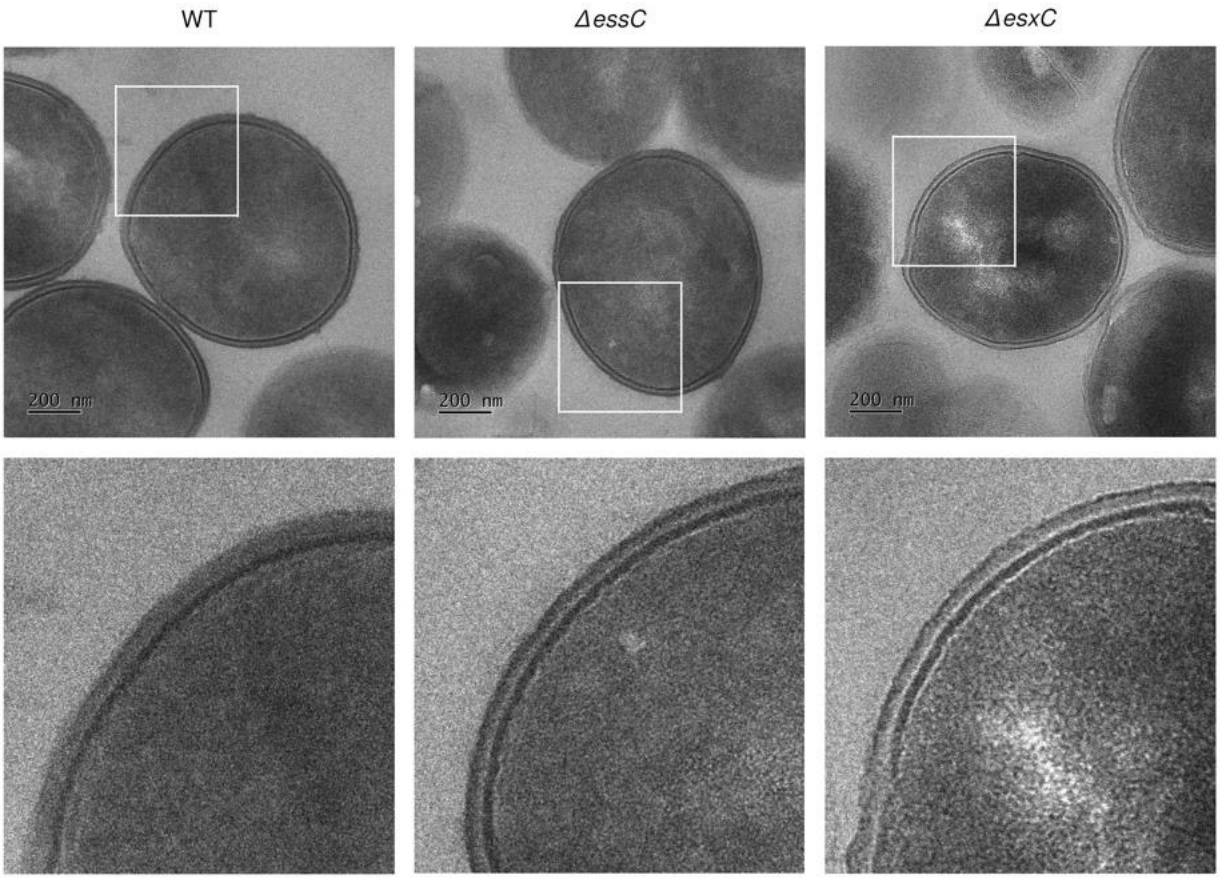

Figure S5. Transmission electron micrographs of *S. aureus* USA300 JE2 WT, Δ*essC* and Δ*esxC* grown to early logarithmic phase

Fig S6

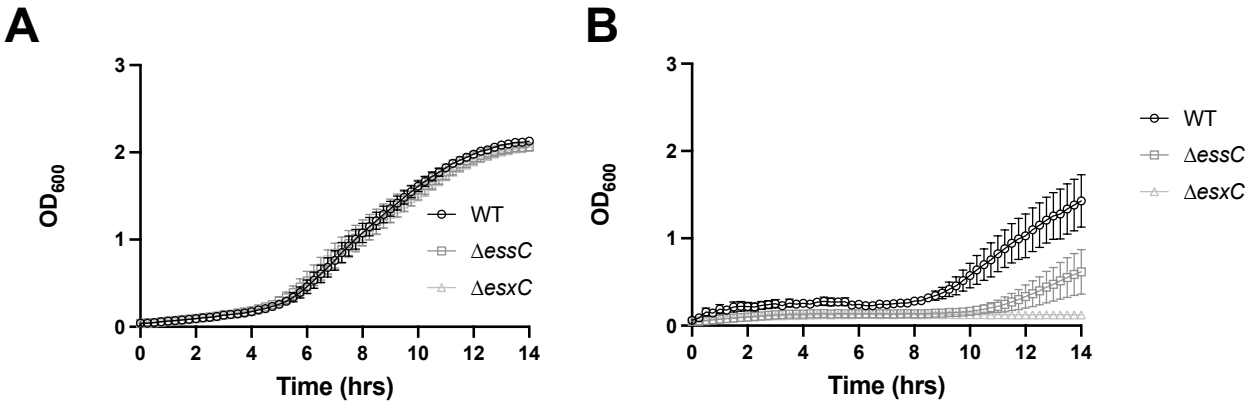

Figure S6. (A) Growth curves of WT, ΔessC and Δ*esxC* in DMEM + FBS. **(B)** Growth curves of WT, Δ*essC* and ΔesxC in DMEM + FBS in the presence of 1µg/ml daptomycin and 1 mM $CaCl_2$. Graphs show mean and SEM of three independent experiments.

Fig S7

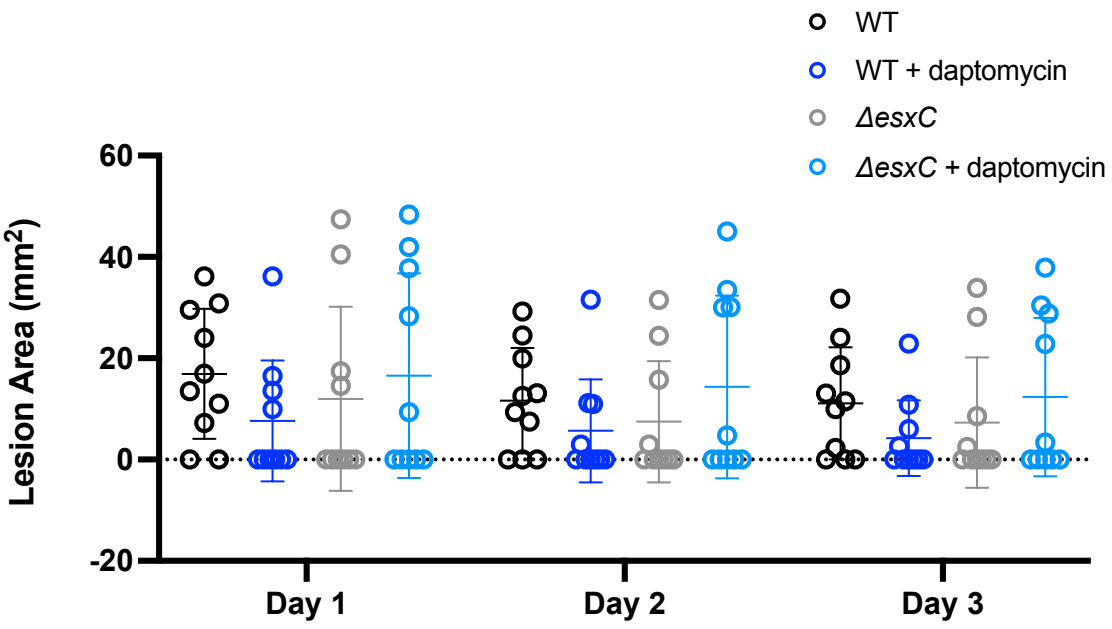

Figure S7 The area of lesions was measured and calculated daily from mice infected with *S. aureus* WT or T7SS mutants. Area of lesions was measured and calculated daily. Graphs show mean ± SD. Two-way ANOVA between groups revealed no significant differences between treatments.

Table S1. **Secreted proteins significantly changed in Δ*esxC* and Δ*essC* mutants relative to WT USA300 JE2. Proteins common to both mutants are in bold.**

	Uniprot ID	log_2 fold change	Adjusted *P* value	Description
USA300 JE2 Δ*esxC* vs USA300 JE2 WT	**A0A0H2XIV9**	**-4.27**	**7.11E-10**	**T7SS protein EssD**
	A0A0H2XHT7	**-2.78**	**7.96E-09**	**Phosphocarrier protein HPr**
	A0A0H2XH98	**-1.75**	**1.34E-07**	**Hydrolase, MutT/nudix family**
	A0A0H2XIK2	**-1.71**	**1.34E-07**	**T7SS protein EsxC**
	A0A0H2XI99	**-1.45**	**0.003045**	**T7SS protein EsxA**
	A0A0H2XFA5	-1.28	4.03E-05	Putative GTP-binding protein
	A0A0H2XEF1	**1.55**	**3.40E-06**	**2-oxoisovalerate dehydrogenase**
	Q2FEF1	**1.63**	**0.000836**	**Isopentenyl-diphosphate delta-isomerase**
	A0A0H2XKB6	**1.90**	**0.00012**	**Uncharacterized protein**
	A0A0H2XH53	2.58	0.042723	Uncharacterized protein
USA300 JE2 Δ*essC* vs USA300 JE2 WT	A0A0H2XI99	-6.59779	1.63E-07	T7SS protein EsxA
	A0A0H2XIV9	-4.27062	7.11E-10	T7SS protein EssD
	A0A0H2XHT7	-2.77719	7.96E-09	Phosphocarrier protein HPr
	A0A0H2XKB6	-2.39392	2.34E-05	Uncharacterized protein
	A0A0H2XH98	-1.74886	1.34E-07	Hydrolase, MutT/nudix family
	A0A0H2XIK2	-1.70544	1.34E-07	T7SS protein EsxC
	A0A0H2XJ55	-1.24877	0.000168	Uncharacterized protein
	Q2FHI5	-1.04906	0.015225	ATP-dependent protease subunit HslV
	Q2FFT2	0.777989	0.026729	Serine protease
	A0A0H2XEF1	1.394088	5.08E-06	2-oxoisovalerate dehydrogenase
	A0A0H2XHA0	1.470262	0.041559	Uncharacterized protein
	A0A0H2XG38	1.580427	1.63E-07	Uncharacterized protein
	Q2FEF1	1.633554	0.000707	Isopentenyl-diphosphate delta-isomerase